1 **Global Soil Consumption of Atmospheric Carbon Monoxide:**

2 **An Analysis Using a Process-Based Biogeochemistry Model**

3 Licheng Liu[1], Qianlai Zhuang[1,2], Qing Zhu[1,3], Shaoqing Liu[1,4], Hella van Asperen[5], Mari

4 Pihlatie[6,7]

[1]Department of Earth, Atmospheric, Planetary Sciences, Purdue University, West Lafayette, IN 47907,

USA

[2]Department of Agronomy, Purdue University, West Lafayette, IN 47907, USA

[3] Climate Sciences Department, Climate & Ecosystem Sciences Division, Lawrence Berkeley National

Laboratory, Berkeley, CA 94720, USA

[4]Department of Earth Sciences, University of Minnesota, Minneapolis, MN, 55455,USA

[5]Institute of Environmental Physics, University of Bremen, Otto-Hahn-Allee 1, Bremen, 28359, Germany

[6]Department of Physics, University of Helsinki, P.O. Box 48, 00014 University of Helsinki, Finland

[7]Department of Forest Sciences, P.O. Box27, 00014 University of Helsinki, Finland

5 *Correspondence to:* Qianlai Zhuang(qzhuang@purdue.edu)

Abstract: Carbon monoxide (CO) plays an important role in controlling the oxidizing capacity of the atmosphere by reacting with OH radicals that affect atmospheric methane (CH_4) dynamics. We develop a process-based biogeochemistry model to quantify CO exchange between soils and the atmosphere with a 5-minute internal time step at the global scale. The model is parameterized using CO flux data from the field and laboratory experiments for eleven representative ecosystem types. The model is then extrapolated to the global terrestrial ecosystems using monthly climate forcing data. Global soil gross consumption, gross production, and net flux of the atmospheric CO are estimated to be from -197 to -180, 34 to 36, and -163 to -145 Tg CO yr^{-1} (1Tg = 10^{12} g), respectively, driven with satellite-based atmospheric CO concentration data during 2000-2013. Tropical evergreen forest, savanna and deciduous forest areas are the largest sinks at 123 Tg CO yr^{-1}. Soil CO gross consumption is sensitive to air temperature and atmospheric CO concentration while gross production is sensitive to soil organic carbon (SOC) stock and air temperature. By assuming that the spatially-distributed atmospheric CO concentrations (~128 ppbv) are not changing over time, global mean CO net deposition velocity is estimated to be 0.16-0.19 mm s^{-1} during the 20th century. Under the future climate scenarios, the CO deposition velocity will increase at 0.0002-0.0013 mm s^{-1} yr^{-1} during 2014-2100, reaching 0.20-0.30 mm s^{-1} by the end of the 21st century, primarily due to increasing temperature. Areas near the equator, Eastern US, Europe and eastern Asia will be the largest sinks due to optimum soil moisture and high temperature. The annual global soil net flux of atmospheric CO is primarily controlled by air temperature, soil temperature, SOC and atmospheric CO concentrations, while its monthly variation is mainly determined by air temperature, precipitation, soil temperature and soil moisture.

1. Introduction

Carbon monoxide (CO) plays an important role in controlling the oxidizing capacity of the atmosphere by reacting with OH radicals (Logan et al., 1981; Crutzen, 1987; Khalil & Rasmussen, 1990; Prather et al., 1995; Prather & Ehhalt, 2001). CO in the atmosphere can directly and indirectly influence the fate of critical greenhouse gases such as methane (CH_4) and ozone (O_3) (Tan and Zhuang, 2012). Although CO itself absorbs only a limited amount of infrared radiation from the Earth, the cumulative

39 indirect radiative forcing of CO may be even larger than that of the third powerful
40 greenhouse gas, nitrous oxide (N_2O, Myhre et al., 2013). Current estimates of global
41 CO emissions from both anthropogenic and natural sources range from 1550 to 2900
42 Tg CO yr^{-1}, which are mainly from anthropogenic and natural direct emissions and from
43 the oxidation of methane and other Volatile Organic Compounds (VOC) (Prather et al.,
44 1995; Khalil et al., 1999; Bergamaschi et al., 2000; Prather & Ehhalt, 2001, Stein et al.,
45 2014). Chemical consumption of CO by atmospheric OH and the biological consumption
46 of CO by soil microbes are two major sinks of the atmospheric CO (Conrad, 1988; Lu &
47 Khalil, 1993; Yonemura et al., 2000; Whalen & Reeburgh, 2001).

48   Soils are globally considered as a major sink for CO due to microbial activities
49 (Whalen and Reeburgh, 2001; King and Weber, 2007). A diverse group of soil microbes
50 including carboxydotrophs, methanotrophs and nitrifiers are capable of oxidizing CO
51 (King and Weber, 2007). Annually, 10-25% of total earth surface CO emissions were
52 consumed by soils (Sanhueza et al., 1998; King, 1999a; Chan & Steudler, 2006). Potter
53 et al. (1996) reported the global soil consumption to be from -50 to -16 Tg CO yr^{-1}
54 (negative values represent the uptake from the atmosphere to soil), by using a single-
55 box model over the upper 5 cm of soils. All existing estimates have large uncertainties
56 and range from -640 to -16 Tg CO yr^{-1} (Sanhueza et al., 1998; King, 1999; Bergamaschi
57 et al., 2000). Similarly, the estimates of CO dry deposition velocities also have large
58 uncertainties and range from 0 to 4.0mm s^{-1} (here positive values are amount of
59 deposition to soils, King, 1999a; Castellanos et al., 2011). Soils also produce CO mainly
60 via abiotic processes such as thermal- and photo-degradation of organic matter or plant
61 materials (Conrad and Seiler, 1985b; Tarr et al., 1995; Schade et al., 1999; Derendorp
62 et al., 2011; Lee et al., 2012; van Asperen et al., 2015; Fraser et al., 2015, Pihlatie et al.,
63 2016), except for a few cases of anaerobic formation. Photo-degradation is identified as
64 radiation-dependent degradation due to absorbing radiation (King et al., 2012).
65 Thermal-degradation is identified as the temperature-dependent degradation of carbon
66 in the absence of radiation and possibly oxygen (Derendorp et al., 2011; Lee et al.,
67 2012; van Asperen et al., 2015; Pihlatie et al., 2016). These major soil CO production
68 processes, together with soil CO consumption processes, have not been adequately
69 modeled in global soil CO budget estimates.

To date, most top-down atmospheric models applied a dry deposition scheme based on the resistance model of Wesely (1989). Such schemes provided a wide range of dry deposition velocities (Stevenson et al., 2006). Only a few models (MOZART-4, Emmons et al., 2010; CAM-chem, Lamarque et al., 2012) have extended their dry deposition schemes with a parameterization for CO and H_2 uptake through oxidation by soil microbes following the work of Sanderson et al. (2003), which itself was based on extensive measurements from Yonemura et al. (2000). Potter et al. (1996) developed a bottom-up model to simulate CO consumption and production at the global scale. This model is a single box model, only considers top 5cm depth of soil and does not have explicit microbial factors, which might have underestimated CO consumption (Potter et al., 1996; King, 1999a). Current bottom-up CO modeling approaches are mostly based on a limited number of CO *in situ* observations or laboratory studies to quantify regional and global soil consumption (Potter et al., 1996; Sanhueza et al., 1998; Khalil et al., 1999; King, 1999a; Bergamaschi et al., 2000; Prather & Ehhalt, 2001). To our knowledge, no detailed process-based model of soil-atmospheric exchange of CO has been published in the recent 15 years. One reason is that there is an incomplete understanding of biological processes of uptake (King & Weber, 2007; Vreman et al., 2011; He and He, 2014; Pihlatie et al., 2016). Another reason is that there is lack of long-term CO flux measurements for different ecosystem types to calibrate and evaluate the models. CO flux measurements are mostly from short-term field observations or laboratory experiments (e.g. Conrad and Seiler, 1985a; Funk et al., 1994; Tarr et al., 1995; Zepp et al., 1997; Kuhlbusch et al., 1998; Moxley and Smith, 1998; Schade et al., 1999; King and Crosby, 2002; Varella et al., 2004; Lee et al., 2012; Bruhn et al., 2013; van Asperen et al., 2015). The first study to report long-term and continuous field measurements of CO flux over grasslands using a micrometeorological eddy covariance (EC) method is Pihlatie et al. (2016).

To improve the quantification of the global soil CO budget for the period 2000-2013 and CO deposition velocity for the 20th and 21st centuries, this study developed a CO dynamics module (CODM) embedded in a process-based biogeochemistry model, the Terrestrial Ecosystem Model (TEM) (Zhuang et al., 2003, 2004, 2007). CODM was then calibrated and evaluated using laboratory experiments and field measurements for

different ecosystem types. The atmospheric CO concentration data from MOPITT (Gille, 2013) were used to drive model simulations from 2000 to 2013. A set of century-long simulations of 1901-2100 were also conducted using the atmospheric CO concentrations estimated with an empirical function (Badr & Probert, 1994; Potter et al., 1996). Finally, the effects of multiple forcings on the global CO consumption and production, including the changes of climate and atmospheric CO concentrations at the global scale were evaluated with the model.

2. Method

2.1 Overview

We first developed a daily soil CO dynamics module (CODM) that considers: (1) soil-atmosphere CO exchange and diffusion process between soil layers, (2) consumption by soil microbial oxidation, (3) production by soil chemical oxidation, and (4) the effects of temperature, soil moisture, soil CO substrate and surface atmospheric CO concentration on these processes. Second, we used the observed soil temperature and moisture to evaluate TEM hydrology module and soil thermal module in order to estimate soil physical variables. Then we used the data from laboratory experiments and CO flux measurements to parameterize the model using the Shuffled Complex Evolution (SCE-UA) method (Duan et al., 1993). Finally, the model was extrapolated to the globe at a 0.5° by 0.5° resolution. We conducted three sets of model experiments to investigate the impact of climate and atmospheric CO concentrations on soil CO dynamics: 1) simulations for 2000-2013 with MOPITT satellite atmospheric CO concentration data; 2)simulations for 1901-2100 with constant atmospheric CO concentrations estimated from an empirical function and the historical climate data (1901-2013) and three future climate scenarios (2014-2100); and 3) Eight sensitivity simulations by changing a) constant CO surface concentrations ± 30%, b) SOC ±5%, c) precipitation ±20% and d) air temperature ± 3°C for each pixel, respectively, while holding other forcing data as they were, during 1999-2000.

2.2 Carbon Monoxide Dynamics Module (CODM)

131   Embedded in TEM (Figure 1), CODM is mainly driven by: (1) soil organic carbon
132   availability based on a carbon and nitrogen dynamics module (CNDM) (Zhuang et al.,
133   2003); (2) soil temperature profile from a soil thermal module (STM) (Zhuang et al.,
134   2001, 2003); and (3) soil moisture profile from a hydrological module (HM) (Bonan,
135   1996; Zhuang et al, 2004). Net exchange of CO between the atmosphere and soil is
136   determined by the mass balance approach (net flux = total production – total oxidation –
137   total soil CO concentration change). According to previous studies, we separated active
138   soils (top 30cm) for CO consumption and production into 1 cm thick layers (King, 1999a,
139   1999b; Whalen & Reeburgh, 2001; Chan & Steudler, 2006). Between the soil layers, the
140   changes of CO concentrations were calculated as:

$$141 \quad \frac{\partial(C(t,i))}{\partial t} = \frac{\partial}{\partial z}\left(D(t,i)\frac{\partial(C(t,i))}{\partial z}\right) + P(t,i) - O(t,i) \quad (1)$$

142   Where $C(t,i)$ is the CO concentration in layer i and at time t, units are mg m^{-3}. z is the
143   depth of the soil, units are m. $D(t,i)$ is the diffusion coefficient for layer i, units are m^2 s^{-1}.
144     $P(t,i)$ is the CO production rate and $O(t,i)$ is the CO consumption rate. The units of
145     $P(t,i)$ and $O(t,i)$ are mg m^{-3} s^{-1}. $D(t,i)$ is calculated using the method from Potter et al.
146   (1996), which are the functions of soil temperature, soil texture and soil moisture. The
147   upper boundary condition is specified as the atmospheric CO concentration, which is
148   estimated by an empirical function of latitude (Potter et al., 1996) or directly measured
149   by the MOPITT satellite during 2000-2013. The lower boundary condition is assumed to
150   have no diffusion exchange with the layer underneath. This partial differential equation
151   (PDE) is solved using the Crank-Nicolson method for less time-step-sensitive solution.
152   CO consumption was modeled in unsaturated soil pores as:

$$153 \quad O(t,i) = V_{max} \cdot f_1(C(t,i)) \cdot f_2(T(t,i)) \cdot f_3(M(t,i)) \quad (2)$$

154   Where V_{max} is the ecosystem specific maximum oxidation rate and was estimated
155   previously ranging from 0.3 to 11.1 µg CO g^{-1} h^{-1} for different ecosystems (Whalen &
156   Reeburgh, 2001). f_i represents the effects of soil CO concentration $C(t,i)$, temperature
157     $T(t,i)$ and moisture $M(t,i)$ on CO soil consumption. Considering CO consumption as
158   the result of microbial activities, we calculated $f_1(C(t,i))$, $f_2(T(t,i))$ and $f_3(M(t,i))$ in a
159   similar way as Zhuang et al. (2004):

$$160 \qquad f_1\big(C(t,i)\big) = \frac{C(t,i)}{C(t,i) + k_{CO}} \qquad (2.1)$$

$$161 \qquad f_2\big(T(t,i)\big) = Q_{10}^{\frac{T(t,i) - T_{ref}}{10}} \qquad (2.2)$$

$$162 \qquad f_3\big(M(t,i)\big) = \frac{(M(t,i) - M_{min})(M(t,i) - M_{max})}{(M(t,i) - M_{min})(M(t,i) - M_{max}) - (M(t,i) - M_{opt})^2} \qquad (2.3)$$

163 Where $f_1\big(C(t,i)\big)$ is a multiplier that enhances oxidation rate with increasing soil CO

164 concentrations using a Michaelis-Menten function with a half-saturation constant k_{CO},

165 and their values were previous estimated ranging from 5 to 51 µl CO l⁻¹ for different

166 ecosystems (Whalen & Reeburgh, 2001); $f_2\big(T(t,i)\big)$ is a multiplier that enhances CO

167 oxidation rates with increasing soil temperature using a Q10 function with Q_{10}

168 coefficients (Whalen & Reeburgh, 2001). T_{ref} is the reference temperature, units are °C

169 (Zhuang et al., 2004, 2013). $f_3\big(M(t,i)\big)$ is a multiplier to estimate the biological limiting

170 effect that diminishes CO oxidation rates if the soil moisture is not at an optimum level

171 (M_{opt}). M_{min}, M_{max} and M_{opt} are the minimum, maximum and optimum volumetric soil

172 moistures of oxidation reaction, respectively. Equation (2.2) will overestimate CO

173 consumption at higher temperature because in reality CO consumption will decrease at

174 higher temperatures than optimum temperature, while f_2 will keep increasing with rising

175 temperature. However, the CO consumption is constrained by CO production, and

176 equation (1) is used to represent this constraint.

177 We modeled the CO production rate ($P(t,i)$) as a process of chemical oxidation

178 constrained by soil organic carbon (SOC) decay (Conrad and Seiler,1985; Potter et al.

179 1996; Jobbagy & Jackson, 2000; van Asperen et al., 2015):

$$180 \qquad P(t,i) = P_r(t,i) \cdot E_{SOC} \cdot C_{SOC}(t) \cdot F_{SOC} \qquad (3)$$

181 Where $P_r(t,i)$ is a reference soil CO production rate which has been normalized to rate

182 at reference temperature (production rate at temperature (t,i) divided by production

183 rate at reference temperature), which is affected by soil moisture and soil temperature

184 (Conrad and Seiler,1985; van Asperen et al., 2015). E_{SOC} is an estimated nominal CO

185 production factor of 3.5 ± 0.9 X 10⁻⁹ mg CO m⁻² s⁻¹ per g SOC m⁻² (to 30 cm surface soil

186 depth) (Potter et al., 1996). $C_{SOC}(t)$ is a SOC content in mg m⁻², which is provided by

187 CNDM module in TEM. F_{SOC} is a constant fraction of top 30cm SOC compared to total
188 amount of SOC, which is 0.33 for shrubland areas, 0.42 for grassland areas and 0.50
189 for forest areas, respectively (Jobbagy & Jackson, 2000). $P_r(t,i)$ was calculated as:

$$P_r(t,i) = \exp\left(f_4\big(M(t,i)\big) \cdot Ea_{ref}/R \cdot \left(\frac{1}{273.15 + PT_{ref}} - \frac{1}{T(t,i) + 273.15} \right) \right) \quad (3.1)$$

$$f_4\big(M(t,i)\big) = \frac{PM_{ref}}{M(t,i) + PM_{ref}} \quad (3.2)$$

192 Where equation (3.1) is derived from Arrhenius equation for chemical reactions and
193 normalized using the reference temperature PT_{ref}. Ea_{ref}/R is the reference activation
194 energy divided by gas constant R, units are K. $f_4\big(M(t,i)\big)$ is the multiplier that reduces
195 activation energy using a regression approach based on laboratory experiment of
196 moisture influences on CO production (Conrad and Seiler,1985). PM_{ref} is the reference
197 volumetric soil moisture, ranging from 0.01 to 0.5 volume/volume (v/v). We assumed
198 thermal-degradation as the main CO producing process due to lack of photo-
199 degradation data and hard to distinguish photo-degradation from observations. In order
200 to reduce the bias from thermal-degradation to total abiotic degradation, the equation
201 (3.1) is parameterized by comparing with total production rate. For instance, $P_r(t,i)$
202 calculation can perfectly fit the experiment results in Van Asperen et al., 2015 with
203 proper PT_{ref}(18°C), Ea_{ref}/R(14000 K) and PM_{ref}(0.5 v/v).

204 CO deposition velocity was modeled in the same way as equation (19.1) in
205 Seinfeld, et al. (1998):

$$v_d = -F_{net}/C_{CO,air} \quad (4)$$

207 Where the v_d is the CO deposition velocity, units are mm s^{-1}; F_{net} is the model
208 estimated CO net flux rate, units are mg CO m^{-2} day^{-1}; $C_{CO,air}$ is the CO surface
209 concentration, units are ppbv. $C_{CO,air}$ can be MOPITT CO surface concentration data or
210 derived CO surface concentrations using the same method as Potter et al. (1996).
211 Positive values of v_d are soil uptake (deposition from air to soils) and negative values
212 are soil emission.

213

214 **2.3 Model Parameterization and Extrapolation**

The model parameterization was conducted in two steps: 1) Thermal and hydrology modules embedded in TEM were revised, calibrated and evaluated by running model with corresponding local meteorological or climatic data at four representative sites, including boreal forest, temperate forest, tropical forest and savanna (Table 1, site No.1 to 4, Figure 2) to minimize model data mismatch in terms of soil temperature and moisture. 2) CODM module was parameterized by running TEM for observational periods with the corresponding local meteorological or climatic data at each reference site (Table 1, Figure 3), and using the Shuffled Complex Evolution Approach in R language (SCE-UA-R) (Duan et al., 1993) to minimize the difference between simulated and observed net CO flux. Eleven parameters including k_{CO}, V_{max}, T_{ref}, Q_{10}, M_{min}, M_{max}, M_{opt}, E_{SOC}, Ea_{ref}/R, PM_{ref} and PT_{ref} were optimized (Table 2). To be noticed, F_{SOC} was not involved in the calibration process. Parameter priors were decided based on previous studies (Conrad & Seiler, 1985; King, 1999b; Whalen & Reeburgh, 2001; Zhuang et al., 2004). SCE-UA-R was used for site No. 6, 8, 10, 11 (Table 1). Each site has been run 50 times using SCE-UA-R with 10000 maximum loops for parameter ensemble, and all of them reached stable state before the end of the loops. For wetlands, the only available data is from site No.12. We used a trial-and-error method to make our simulated results in the range of observed flux rates, with a 10% tolerance. For tropical sites, since tropical savanna vegetation type is a combination type of tropical forest and grassland in our model, we first used Site No. 13 to set priors to fit the experiment results with a 10% tolerance and then evaluated by running our model comparing with site No.7 results. Site No. 9 and 5 were used to evaluate our model results for temperate forest and grassland. Besides the observed climatic and soil property data, we used ERA-Interim reanalysis data from The European Centre for Medium-Range Weather Forecasts (ECMWF) (Dee et al., 2011), AmeriFlux observed meteorology data (http://ameriflux.lbl.gov/) and reanalysis climatic data from Climatic Research Unit (CRU, Harris et al., 2013) to fill the missing environmental data. To sum up, parameters for various ecosystem types in Table 2 were the final results of our parameterization. Model parameterization was conducted for ecosystem types including boreal forest, temperate coniferous forest, temperate deciduous forest, and grassland using SCE-UA-R. Tropical forest and wet tundra used

246   a trial-and-error method to adjust parameters letting simulation results best fit the lab
247   data. Due to limited data availability, we assumed temperate evergreen broadleaf forest
248   having the same parameters as temperate deciduous forest.

249

250   **2.4 Data Organization**

251   To get spatially and temporally explicit estimates of CO consumption, production
252   and net flux at the global scale, we used the data of land cover, soils, climate and leaf
253   area index (LAI) from various sources at a spatial resolution of 0.5° latitude X 0.5°
254   longitude to drive TEM. The land cover data include potential vegetation distribution
255   (Melillo et al., 1993) and soil texture (Zhuang et al., 2003), which were used to assign
256   vegetation- and texture-specific parameters to each grid cell.

257   For the simulation of the period 1901-2013, monthly air temperature, precipitation,
258   clouds fraction and vapor pressure data sets from CRU were used to estimate the soil
259   temperature, soil moisture and SOC with TEM (Figure 4). Monthly LAI data from TEM
260   were required to simulate soil moisture (Zhuang et al., 2004). During this period time,
261   we used an empirical function of latitude, which was derived from the observed
262   latitudinal distribution of tropospheric carbon monoxide (Badr and Probert, 1994) to
263   calculate static CO surface concentration distribution (equation (7), Potter et al., 1996):

264    $$C_{CO,air} = 82.267856 + 0.8441503L + 1.55934 \times 10^{-2}L^2 + 2.37 \times 10^{-5}L^3 - $$

265    $$2.3 \times 10^{-6}L^4 \qquad\qquad (5)$$

266   Where $C_{CO,air}$ is the derived surface CO concentration (ppbv), L represents
267   latitude which is negative degrees for southern hemisphere and positive degrees for
268   northern hemisphere. We also used the atmospheric CO data from MOPITT satellite
269   during 2000-2013 (Figure 5). We averaged day-time and night-time monthly mean
270   retrieved CO surface level 3 data (variables mapped on 0.5° latitude X 0.5° longitude
271   grid scales with monthly time step, Gille, 2013) to represent the CO surface
272   concentration level in each month. The missing pixels were fixed by the average of
273   pixels which had values and were inside 1.5 times of the distance between this missing
274   pixel and the nearest pixel with values. These global mean values shown in Figure 5 do
275   not include ocean surfaces, thus there are differences between our surface CO

276 concentration results and Yoon and Pozzer's report in 2014, which is as low as 99.8ppb.
277 From 2014 to 2100, we used Intergovernmental Panel on Climate Change (IPCC) future
278 climate scenarios from Representative Concentration Pathways (RCPs) climate forcing
279 data sets RCP2.6, RCP4.5 and RCP8.5 (Figure 6). RCP2.6, 4.5 and 8.5 datasets are
280 future climate projections with anthropogenic greenhouse gas emission radiative forcing
281 of 2.6 W m^{-2}, 4.5 W m^{-2} and 8.5 W m^{-2}, respectively, by 2100. Since RCPs did not have
282 water vapor pressure data, we used the specific humidity and sea level air pressure
283 from the RCPs and elevation of surface to estimate the monthly surface vapor pressure
284 (Seinfeld & Pandis, 1998).
285
286 **2.5 Model Experiment Design**

287 We conducted two sets of core simulations and eight sensitivity test simulations
288 for a historical period. The two core sets of simulations were driven with MOPITT CO
289 surface concentrations data for the period 2000-2013 (experiment E1) and with spatially
290 distributed CO surface concentrations assuming as constant over time estimated from
291 an empirical function of latitude for the period 1901-2100 (experiment E2), respectively.
292 Specifically, in experiment E2 we used the CRU climate forcing for the historical period
293 1901-2013 and the climate data of RCP2.6, RCP4.5 and RCP8.5 for different future
294 scenarios to examine the responses of CO flux to changing climates. Eight sensitivity
295 simulations were driven with varying different forcing variables while keeping others as
296 they were: 1) with constant CO surface concentrations ± 30%, 2) SOC ±5%, 3)
297 precipitation ±20% and 4) air temperature ± 3°C for each pixel, respectively, during
298 1999-2000 (E3).
299
300 **3. Results**

301 **3.1 Site Evaluation**

302 Both the magnitude and variation of the simulated soil temperature and moisture
303 from cold areas to warm areas compared well to the observations (Figure. 2). The
304 magnitude of the simulated CO flux is comparable and correlated with the observations
305 (r is about 0.5, p-value < 0.001, Figures 3, a2, b2, c2, d2). Estimated CO fluxes for

306 different ecosystem types range from -28.4 to 1.7 mg CO m^{-2} day^{-1}, and the root mean

307 square error (RMSE) between simulation and observation at all sites is below 1.5 mg

308 CO m^{-2} day^{-1}. RMSE for site No. 7 is bigger than 2.0 mg CO m^{-2} day^{-1} when compared

309 with transparent chamber observations.   For boreal forest site, we only had 8

310 acceptable points in 1994 and 1996 (Figure 3c2).

311

3.2 Global Soil CO Dynamics During 2000-2013

313   Using the MOPITT CO surface concentration data during 2000-2013 (E1), the

314 estimated mean soil CO consumption, production and net flux (positive values indicate

315 CO emissions from soils to the atmosphere) are from -197 to -180, 34 to 36 and -163 to

316 -145 Tg CO yr^{-1}, respectively (Figure 7a). Consumption is about 4 times larger than

317 production. The annual consumption and net flux trends follow the atmospheric CO

318 concentration trends (Figure 5b, Figure 7a), with a small interannual variability (<10%).

319 The latitudinal distributions of consumption, production and net fluxes share the same

320 spatial pattern. Around 20°S-20°N and 20-60N° are the largest and second largest

321 areas for production and consumption, while the 45°S-45°N area accounts for nearly 90%

322 of the total consumption and production (Figure 7b, Table 3). The Southern and

323 Northern Hemispheres have 41% and 59% of the total consumption, and 47% and 53%

324 of the total production, respectively (Table 3).   The highest rates of consumption and

325 production are located in areas close to the equator, and consumption from areas such

326 as eastern US, Europe and eastern Asia also is high (>-1000 mg m^{-2} yr^{-1}) (Figure 8a, b).

327 Global soils serve as an atmospheric CO sink (Figure 8c). Some areas, such as

328 western US and southern Australia, are CO sources, all of which are grasslands or

329 experiencing dry climate. Tropical evergreen forests are the largest sinks, consuming 86

330 Tg CO yr^{-1}, and tropical savanna and deciduous forest are second and third largest

331 sinks, consuming a total of 37 Tg CO yr^{-1} (Table 4). These three ecosystems account

332 for 66% of the total consumption. Tropical evergreen forests are also the largest source

333 of soil CO production, producing 16 Tg CO yr^{-1}, while tropical savanna has a

334 considerable production of 6 Tg CO yr^{-1} (Table 4). Moreover, tropical areas, including

335 forested wetlands, forested floodplain and evergreen forests, are most efficient for CO

336 consumption, ranging from -18 to -13 mg CO m^{-2} day$^{-1.}$ They are also the most efficient

337 for CO production at over 2 mg CO m^{-2} day^{-1} (Table 4, calculated by fluxes divided by
338 area).

339

340 **3.3 Global Soil CO Dynamics During 1901-2100**

341   Using the constant CO surface concentration, the estimated global mean CO
342 deposition velocities are 0.16-0.19 mm s^{-1} for the period 1901-2013. For the period
343 2014-2100, deposition velocities are 0.18-0.21, 0.18-0.24 and 0.17-0.31 for RCP2.6, 4.5
344 and 8.5 scenarios, respectively (Figure 9). During 2014-2100, there are significant
345 trends of increasing deposition velocities for nearly all scenarios (Figure 9). The rates of
346 increasing are 0.0002, 0.0005 and 0.0013 mm s^{-1} yr^{-1}, and will reach 0.20, 0.23 and
347 0.30 mm s^{-1} by the end of the 21st century for the RCP2.6, RCP4.5 and RCP8.5
348 scenarios, respectively (Figure 9). These increasing trends are similar to air
349 temperature increasing trends (Figure 6a). Global distribution patterns of CO deposition
350 velocity are similar to net flux distribution for the period 2000-2013 but there are
351 significant differences among 1901-2013, RCP2.6, RCP4.5 and RCP8.5 scenarios
352 (Figure 10). Deposition velocities are increasing from RCP2.6 to RCP8.5 and larger
353 than in the historical periods in areas near the equator (Figure 10). Areas near the
354 equator and eastern Asia become big sinks of atmospheric CO, while northeastern US
355 becomes a small source in the 21st century (Figure 10). Different vegetation types have
356 a large range of deposition velocity, from 0.008 to 1.154 mm s^{-1} (Table 4). The tropical
357 forested wetland, tropical forested floodplain and tropical evergreen forest have top
358 three largest deposition velocity of 1.154, 1.117 and 0.879 mm s^{-1}, respectively, while
359 desert, short grasslands, and wet tundra have the smallest deposition velocity 0.008,
360 0.010 and 0.015 mm s^{-1}, respectively.

361

362 **3.4 Sensitivity test**

363   Eight sensitivity tests have been conducted for the 1999-2000 period, including
364 changing atmospheric CO by ±30%, SOC by ±5%, precipitation by ±30% and air
365 temperature by ±3°C for each pixel (Table 5). Soil CO consumption is most sensitive

366 (changing 29%) to air temperature while production is most sensitive to both air

367 temperature (changing up to 36%) and SOC (5%). The net CO fluxes have the similar

368 sensitivities as consumption. Annual CO consumption, production and net flux follow the

369 change of air temperature (Table 5). In addition, a 30% change in precipitation will not

370 lead to large changes in CO flux (< 3%).

371

372 **4. Discussion**

373 **4.1 Comparison with Other Studies**

374   Previous studies estimated a large range of global CO consumption from -16 to -

375 640 Tg CO yr^{-1}. Our estimates are from -197 to -180 Tg CO yr^{-1} for for 2000-2013 using

376 MOPITT satellite CO surface concentration data. Previous studies also provided a large

377 range for CO production from 0 to 7.6 mg m^{-2} day^{-1} (reviewed in Pihlatie et al., 2016).

378 Our results showed averaged CO production ranging from 0.01 to 2.29 mg m^{-2} day^{-1}.

379 Previously reported CO deposition velocities for different vegetation types range from

380 0.0 to 4.0 mm s^{-1} while our results showed an averaged CO deposition velocity ranging

381 from 0.006 to 1.154 mm s^{-1} for different vegetation types. The large uncertainty of these

382 estimates is mainly due to a different consideration of the microbial activities, the depth

383 of the soil, and the parameters in the model. In contrast to the estimates of -57 to -16 Tg

384 CO yr^{-1} which were based on top 5 cm soils (Potter et al., 1996), our estimates

385 considered 30cm soils, just as used in Whalen & Reeburgh (2001). In addition, we

386 used a thinner layer division (1cm each layer) for diffusion process, and used the Crank-

387 Nicolson method to solve partial differential equations to avoid time step influences. We

388 also included the microbial CO oxidation process to remove the CO from soils and the

389 effects of soil moisture, soil temperature, vegetation type and soil CO substrate on

390 microbial activities. Our soil thermal, soil hydrology and carbon and nitrogen dynamics

391 simulated in TEM provided carbon substrate spatially and temporally for estimating soil

392 CO dynamics. Overall, although a few previous studies have examined the long-term

393 impacts of climate, land use and nitrogen depositions on CO dynamics (Chan &

394 Steudler, 2006, Pihlatie et al., 2016), the global prediction of soil CO dynamics still has
395 a large uncertainty.

396

397 **4.2 Major Controls to Soil CO Dynamics**

398   Sensitivity tests indicate that consumption is normally much larger than CO
399 production so that the former will determine the dynamics of the net flux (Table 5).
400 Model being sensitive to air temperature explains the small increasing trends after the
401 1960s, the significant increasing trend in the 21st century and the large sinks over
402 tropical areas (Table 5, Figure 9). SOC did not directly influence CO consumption. For
403 instance, increasing SOC led to an increase in soil CO substrate, implying that more CO
404 in soils can be consumed. To be noticed, an extra 3 Tg CO yr^{-1} was taken up from the
405 atmosphere to soils in sensitivity test when SOC increasing by 5% (Table 5), which will
406 be discussed in detail in Section 4.3. CO surface concentrations will only influence the
407 uptake rate and soil CO substrate concentrations, thus influencing the soil CO
408 consumption rate.

409   Annual CO consumption and net flux have a similar correlation coefficient with
410 forcing variables and both are significantly correlated with air temperature, soil
411 temperature SOC and atmospheric CO concentration (R > 0.91 globally, Table 6).
412 Increasing temperature will increase microbial activities, while more SOC will increase
413 soil CO substrate level. Annual CO consumption and net flux have low correlations with
414 annual precipitation and soil moisture, especially at 45°N-45°S (R<0.54 Table 6).
415 Annual CO production is strongly correlated with annual mean SOC, air temperature
416 and soil temperature (R>0.91), while is less correlated with precipitation, soil moisture
417 and atmospheric CO concentration. Meanwhile, the monthly CO consumption,
418 production and net flux are well correlated with air temperature, soil temperature,
419 precipitation, and soil moisture (R>0.69 globally Table 6). The soil moisture is
420 significantly influenced by temperature at a monthly time step since increasing
421 temperature would induce higher evapotranspiration. Monthly CO consumption,
422 production and net flux have low correlations with SOC because it will not change
423 greatly within a month.

424   The R between annual soil CO consumption and atmospheric CO concentration
425   is 0.91 at the global scale because the atmospheric CO concentration, air temperature,
426   and soil temperature dominate the annual consumption rate. At monthly scale, this R is
427   -0.48 because global atmospheric CO concentrations are high in winter and low in
428   summer while the simulated soil CO consumption shows an opposite monthly variation
429   (Table 6, Figure 11), suggesting that other factors such as precipitation, air temperature,
430   and soil temperature are major controls for monthly CO fluxes.

431

432   **4.3. Model Uncertainties and Limitations**

433   There are a number of limitations, contributing to our simulation uncertainties.
434   First, due to lacking long-period observational data of CO flux and associated
435   environmental factors, the model parameterization can only be conducted for 4
436   ecosystem types including boreal forest, temperate coniferous forest, temperate
437   deciduous forest and grassland. Tropical forest calibration is only conducted using a
438   very limited amount of lab experiment data, but tropical areas are hotspots for CO soil-
439   atmosphere exchanges. Besides, tropical forest SOC for top 30cm can be really high
440   according to observations. TEM model may underestimate the top 30cm SOC, which
441   will underestimate production rates, especially in tropical regions. Tropical regions
442   typically have high temperature during the whole year, which may result in
443   overestimation of CO consumption using equation (2.2). The large deviation for tropical
444   savanna (which is mosaic of tropical forest and grassland ecosystems) may be due to
445   using outside air temperature to represent inside air temperature of transparent
446   chamber observations (Varella et al., 2004), and uncertain tropical forest
447   parameterization. Second, we used the conclusion from van Asperen et al. (2015) and
448   only considered the thermal-degradation process for CO production in this study. Photo-
449   degradation process and biological formation process were not considered due to
450   lacking understanding of these processes. Third, the static CO surface concentration
451   derived from the empirical function is lower than MOPITT CO surface concentration,
452   which will lead to underestimation of CO deposition velocity during 1901-2100. Fourth,
453   from sensitivity test (Table 5) we notice that SOC increasing (5%) resulted in a net flux
454   increase (2.57%). The SOC increase enhanced CO production (Equation 3), CO

455 concentrations (Equation 1), and CO oxidation (Equation 2). When the change of total

456 oxidation is larger than the difference between the change of total production and the

457 change of total soil CO concentration (Equation 1), the estimate of the net flux change is

458 negative (from atmosphere to soil) using a mass balance approach (Section 2.2),

459 leading to a 2.57% increase in net flux in our SOC sensitive test. This is due to the fact

460 that CO production (Equation 3) is calculated independently from oxidation calculation

461 (Equation 2). This will not influence our other results since SOC varies slightly during

462 our simulation periods with only a 3% increase from 1900 to 2013 (Figure 4d) and up to

463 a 4% increase from 2014 to 2100 (Figure 6g). This artifact problem in SOC sensitivity

464 test can be alleviated using a very fine time step (e.g., 1 second), because CO

465 concentrations will change slightly within the short time, allowing net flux roughly equals

466 the difference between production and oxidation within the short time step. If the change

467 of production is bigger than the change of oxidation, the change of net flux will be

468 positive, leading to a decrease of deposit to soil. The downside is that running the

469 model at one second time step will require significantly high computing time. Fifth, our

470 model structure still has a large potential to improve. In this study we divided the top

471 30cm soil into 30 layers (layer thickness dz=1cm), but finer division will increase the

472 accuracy (Figure 12). We chose dz=1cm because if dz>1cm, the model vertical CO

473 concentration profile will deviate from reality and diffusion process will be influenced

474 significantly. If dz<1cm, it will need much more computing time but don't have much

475 improvement compared to dz=1cm (Figure 12a-e). We notice that the 30-layer division

476 well represents soil CO concentration profile not only for the days with soil CO net

477 uptake, but also for the days with CO net emission (Figure 12c, f). Sixth, Michaelis-

478 Menten function (equation 2.1) is used in this model and we notice that k_{CO} is normally

479 much larger than $C(t,i)$ in those days of net soil uptake (over ten times larger, Figure

480 12). However, we can't simplify equation (2.2) to $f_1\big(C(t,i)\big) = \frac{C(t,i)}{k_{CO}}$ since CO

481 concentrations in soils can be larger than in the atmosphere in the days of net

482 emissions and $C(t,i)$ may be close to k_{CO}, which may lead to overestimation of CO

483 oxidation (Figure 12f). Finally, although we focused on natural ecosystems in this study,

484 land-use change, agriculture activity, and nitrogen deposition also affect the soil CO

485 consumption and production (King, 2002; Chan & Steudler, 2006). For instance, soil CO

486 consumption in agriculture ecosystems is 0 to 9 mg CO m^{-2} day^{-1} in Brazil (King &
487 Hungria, 2002). We used grass land or forest ecosystem to represent agriculture areas
488 in CODM module. Our future study shall include these processes and factors.

489

490 **5. Conclusions**

491   We analyzed the magnitude, spatial pattern, and the controlling factors of the
492 atmosphere-soil CO exchanges at the global scale for the 20th and 21st centuries using
493 a process-based biogeochemistry model. Major processes include atmospheric CO
494 diffusion into soils, microbial oxidation removal of CO, and CO production through
495 chemical reaction. We found that air temperature and soil temperature play a dominant
496 role in determining annual soil CO consumption and production while precipitation, air
497 temperature, and soil temperature are the major controls for the monthly consumption
498 and production. Atmospheric CO concentrations are important for annual CO
499 consumption. We estimated that the global annual CO consumption, production and net
500 fluxes for 2000-2013 are from -197 to -180, 34 to 36 and -163 to -145 Tg CO yr^{-1},
501 respectively, when using a MOPITT CO surface concentration data. Tropical evergreen
502 forest, savanna and deciduous forest areas are the largest sinks accounting for 66% of
503 the total CO consumption, while the Northern Hemisphere consumes 59% of the global
504 total. During the 20th century, the estimated CO deposition velocity is 0.16-0.19 mm s^{-1}.
505 The predicted CO deposition velocity will reach 0.20-0.30 mm s^{-1} in the 2090s, primarily
506 because of increasing air temperature. The areas near the equator, eastern Asia,
507 Europe and eastern US will become the sink hotspots because they have warm and
508 moist soils. This study calls for long-period observations of CO flux for various
509 ecosystem types and projection of atmospheric CO surface concentrations from 1901-
510 2100 to improve future estimates of global soil CO consumption. The effects of land-use
511 change, agriculture activities, nitrogen deposition, photo-degradation and biological
512 formation shall also be considered to improve future quantification of soil CO fluxes.

513

514

515 **Acknowledgment**

516   This study is supported through projects funded to Q.Z. by Department of Energy

517 (DE-SC0008092 and DE-SC0007007) and the NSF Division of Information and

518 Intelligent Systems (NSF-1028291). The supercomputing resource is provided by

519 Rosen Center for Advanced Computing at Purdue University. We acknowledge Dr.

520 Stephen C. Whalen made the observational CO flux data available to this study. We are

521 also grateful to University of Tuscia (dep. DIBAF), Italy, and their affiliated members, for

522 their help and the use of their field data.

References:

Badr, O., & Probert, S. D.:Carbon monoxide concentration in the Earth's atmosphere. Applied Energy, doi:10.1016/0306-2619(94)90035-3,1994

Badr, O., & Probert, S. D.: Sinks and environmental impacts for atmospheric carbon monoxide, Applied Energy. doi:10.1016/0306-2619(95)98803-A,1995

Bartholemew, G.W., Alexander, M.: Soils as a sink for atmospheric carbon monoxide, Science 212, 1389-1391, doi:10.1126/science.212.4501.1389, 1981

Bartholomew, G. W., & Alexander, M.: Notes. Microorganisms responsible for the oxidation of carbon monoxide in soil. Environmental Science & Technology. American Chemical Society (ACS), doi:10.1021/es00099a013, 1982

Bender, M., & Conrad, R.: Microbial oxidation of methane, ammonium and carbon monoxide, and turnover of nitrous oxide and nitric oxide in soils, Biogeochemistry, Springer Nature, doi:10.1007/bf00002813, 1994

Bergamaschi, P., Hein, R., Heimann, M., & Crutzen, P. J.: Inverse modeling of the global CO cycle: 1. Inversion of CO mixing ratios, Journal of Geophysical Research: Atmospheres, doi:10.1029/1999jd900818, 2000

Bonan, G.: A Land Surface Model (LSM Version 1.0) for Ecological, Hydrological, and Atmospheric Studies: Technical Description and User's Guide, UCAR/NCAR, doi:10.5065/d6df6p5x, 1996

Bourgeau-Chavez, L.L., Garwood, G.C., Riordan, K., Koziol, B.W., Slawski, J.,: Development of calibration algorithms for selected water content reflectometry probes for burned and nonburned organic soils of Alaska. Int. J. Wildland Fire 19, 961e975, doi:10.1071/wf07175, 2012

Bruhn, D., Albert, K. R., Mikkelsen, T. N., & Ambus, P.: UV-induced carbon monoxide emission from living vegetation. Biogeosciences, Copernicus GmbH, doi:10.5194/bg-10-7877-2013, 2013

Castellanos, P., Marufu, L. T., Doddridge, B. G., Taubman, B. F., Schwab, J. J., Hains, J. C., … Dickerson, R. R.: Ozone, oxides of nitrogen, and carbon monoxide during pollution events over the eastern United States: An evaluation of emissions and vertical mixing, Journal of Geophysical Research Atmospheres, 116(16), doi:10.1029/2010JD014540, 2011

Chan, A. S. K., & Steudler, P. A.: Carbon monoxide uptake kinetics in unamended and long-term nitrogen-amended temperate forest soils. FEMS Microbiology Ecology, 57(3), 343–354, doi:10.1111/j.1574-6941.2006.00127.x, 2006

Conrad, R., & Seiler, W.: Role of Microorganisms in the Consumption and Production of Atmospheric Carbon Monoxide by Soil. Appl. Environ, Microbiol., 40(3), 437–445. Retrieved from http://aem.asm.org/cgi/content/abstract/40/3/437, 1980

Conrad, R., & Seiler, W.: Arid soils as a source of atmospheric carbon monoxide, Geophysical Research Letters, doi:10.1029/gl009i012p01353, 1982

558 Conrad, R., & Seiler, W.: Characteristics of abiological carbon monoxide formation from soil organic
559 matter, humic acids, and phenolic compounds, Environmental Science & Technology, American Chemical
560 Society (ACS), doi:10.1021/es00142a004, 1985

561 Conrad, R., Meyer, O., & Seiler, W.: Role of carboxydobacteria in consumption of atmospheric carbon
562 monoxide by soil, Applied and Environmental Microbiology, 42(2), 211–215, 1981

563 Crutzen, P. J., & Giedel, L. T.: A two-dimensional photochemical model of the atmosphere. 2: The
564 tropospheric budgets of anthropogenic chlorocarbons CO, CH4, CH3Cl and the effect of various NOx
565 sources on tropospheric ozone, J. Geophys. Res., 88(Cll), 6641–6661. doi:10.1029/JC088iC11p06641,
566 1983

567 Crutzen, P.J.: Role of the tropics in atmospheric chemistry, The Geophysiology of Amazonia Vegetation
568 Climate Interaction (Dickinson RE, ed.), pp 107–131. John Wiley, New York, 1987

569 Daniel, J. S., & Solomon, S.: On the climate forcing of carbon monoxide, Journal of Geophysical
570 Research-Atmospheres, 103(D11), 13249–13260. doi:10.1029/98JD00822, 1988

571 Dee, D. P., Uppala, S. M., Simmons, A. J., Berrisford, P., Poli, P., Kobayashi, S., … Vitart, F.: The ERA-
572 Interim reanalysis: configuration and performance of the data assimilation system, Quarterly Journal of
573 the Royal Meteorological Society, doi:10.1002/qj.828, 2011

574 Dentener, F., Drevet, J., Lamarque, J. F., Bey, I., Eickhout, B., Fiore, A. M., … Wild, O.: Nitrogen and
575 sulfur deposition on regional and global scales: A multimodel evaluation, Global Biogeochemical
576 Cycles, 20(4), doi:10.1029/2005GB002672, 2006

577 Derendorp, L., Quist, J. B., Holzinger, R., & Röckmann, T.: Emissions of H2 and CO from leaf litter of
578 Sequoiadendron giganteum, and their dependence on UV radiation and temperature, Atmospheric
579 Environment, 45(39), 7520–7524. doi:10.1016/j.atmosenv.2011.09.044, 2011

580 Duan, Q. Y., Gupta, V. K., & Sorooshian, S.: Shuffled complex evolution approach for effective and
581 efficient global minimization, Journal of Optimization Theory and Applications, 76(3), 501–521.
582 doi:10.1007/BF00939380, 1993

583 Duggin, J. A., & Cataldo, D. A.: The rapid oxidation of atmospheric CO to CO2 by soils, Soil Biology and
584 Biochemistry, 17(4), 469–474, doi:10.1016/0038-0717(85)90011-2, 1985

585 Emmons, L. K., Walters, S., Hess, P. G., Lamarque, J.-F., Pfister, G. G., Fillmore, D., … Kloster, S.:
586 Description and evaluation of the Model for Ozone and Related chemical Tracers, version 4 (MOZART-
587 4), Geoscientific Model Development, 3(1), 43–67. doi:10.5194/gmd-3-43-2010, 2010

588 Fenchel, T., King, G. M., & Blackburn, T. H.: Bacterial biogeochemistry: the ecophysiology of mineral
589 cycling, Bacterial biogeochemistry (p. 307 pp). doi:10.1016/B978-0-12-415836-8.00012-8, 1988

590 Ferenci, T., Strom, T., & Quayle, J. R.: Oxidation of carbon monoxide and methane by Pseudomonas
591 methanica, Journal of General Microbiology, 91(1), 79–91. doi:10.1099/00221287-91-1-79, 1975

592 Fisher, M. E.: Soil-atmosphere Exchange of Carbon Monoxide in Forest Stands Exposed to Elevated and
593 Ambient CO2 (Doctoral dissertation), 2003

594 Fraser, W. T., Blei, E., Fry, S. C., Newman, M. F., Reay, D. S., Smith, K. A., & McLeod, A. R.: Emission of
595 methane, carbon monoxide, carbon dioxide and short-chain hydrocarbons from vegetation foliage under
596 ultraviolet irradiation, Plant, Cell and Environment, 38(5), 980–989. doi:10.1111/pce.12489, 2015

597 Funk, D. W., Pullman, E. R., Peterson, K. M., Crill, P. M., & Billings, W. D.: Influence of water table on
598 carbon dioxide, carbon monoxide, and methane fluxes from Taiga Bog microcosms, Global Biogeochem.
599 Cycles, 8(3), 271–278. doi:10.1029/94gb0122, 1994

600 Galbally, I., Meyer, C. P., Wang, Y. P., & Kirstine, W.: Soil-atmosphere exchange of CH4, CO, N2O and
601 NOx and the effects of land-use change in the semiarid Mallee system in Southeastern Australia, Global
602 Change Biology, 16(9), 2407–2419, doi:10.1111/j.1365-2486.2010.02161.x, 2010

603 Gille, J.: MOPITT Gridded Monthly CO Retrievals (Near and Thermal Infrared Radiances) - Version 6
604 [Data set], NASA Langley Atmospheric Science Data Center. doi:10.5067/TERRA/MOPITT/DATA301,
605 2013

606 Gödde, M., Meuser, K., & Conrad, R.: Hydrogen consumption and carbon monoxide production in soils
607 with different properties, Biology and Fertility of Soils, 32(2), 129–134, doi:10.1007/s003740000226, 2000

608 Guthrie, P. D.: The CH4- CO - OH conundrum: A simple analytic approach, Global Biogeochemical
609 Cycles, doi:10.1029/gb003i004p00287, 1989

610 Hardy, K. R., & King, G. M.: Enrichment of High-Affinity CO Oxidizers in Maine Forest Soil. Applied and
611 Environmental Microbiology, 67(8), 3671–3676, doi:10.1128/AEM.67.8.3671-3676.2001, 2001

612 Harris, I., Jones, P. D., Osborn, T. J., & Lister, D. H.: Updated high-resolution grids of monthly climatic
613 observations - the CRU TS3.10 Dataset, International Journal of Climatology, doi:10.1002/joc.3711, 2013

614 He, H., & He, L.: The role of carbon monoxide signaling in the responses of plants to abiotic
615 stresses, Nitric Oxide : Biology and Chemistry / Official Journal of the Nitric Oxide Society, 42, 40–3.
616 doi:10.1016/j.niox.2014.08.011, 2014

617 Heichel, G. H.: Removal of Carbon Monoxide by Field and Forest Soils1, Journal of Environment Quality,
618 American Society of Agronomy, doi:10.2134/jeq1973.00472425000200040001x, 1973

619 Jobbagy, E. G., & Jackson, R.: The vertical Distribution of soil organic carbon and its relation to climate
620 and vegetation, Ecological Applications, 10:2(April), 423–436, doi:10.2307/2641104, 2000

621 Jones, R. D., & Morita, R. Y.: Carbon monoxide oxidation by chemolithotrophic ammonium
622 oxidizers, Canadian Journal of Microbiology, 29(11), 1545–1551, doi:10.1139/m83-237, 1983

623 Khalil, M. A. ., Pinto, J. ., & Shearer, M.: Atmospheric carbon monoxide, Chemosphere - Global Change
624 Science, Elsevier BV, doi:s1465-9972(99)00053-7,1999

625 Khalil, M. A. K., & Rasmussen, R. A.: The global cycle of carbon monoxide: Trends and mass
626 balance, Chemosphere, 20(1–2), 227–242, doi:10.1016/0045-6535(90)90098-E, 1990

627 King, G. M.: Attributes of Atmospheric Carbon Monoxide Oxidation by Maine Forest Soils, Appl. Environ.
628 Microbiol., 65(12), 5257–5264, 1999

629   King, G. M.: Characteristics and significance of atmospheric carbon monoxide consumption by soils,
630   Chemosphere, 1, 53–63, doi:10.1016/S1465-9972(99)00021-5, 1999a

631   King, G. M.: Land use impacts on atmospheric carbon monoxide consumption by soils, Global
632   Biogeochemical Cycles, 14(4), 1161–1172, doi:10.1029/2000GB001272, 2000

633   King, G. M., & Crosby, H.: Impacts of plant roots on soil CO cycling and soil-atmosphere CO
634   exchange, Global Change Biology, 8(11), 1085–1093, doi:10.1046/j.1365-2486.2002.00545.x, 2002

635   King, G. M., & Hungria, M.: Soil-atmosphere CO exchanges and microbial biogeochemistry of CO
636   transformations in a Brazilian agricultural ecosystem, Applied and Environmental Microbiology, 68(9),
637   4480–4485, doi:10.1128/AEM.68.9.4480-4485.2002, 2002

638   King, G. M., & Weber, C. F.: Distribution, diversity and ecology of aerobic CO-oxidizing bacteria, Nature
639   Reviews, Microbiology, 5(2), 107–18, doi:10.1038/nrmicro1595, 2007

640   King, J. Y., Brandt, L. A., & Adair, E. C.: Shedding light on plant litter decomposition: advances,
641   implications and new directions in understanding the role of photodegradation, Biogeochemistry, 111(1–
642   3), 57–81, doi:10.1007/s10533-012-9737-9, 2012

643   Kisselle, K. W., Zepp, R. G., Burke, R. A., De Pinto, A. S., Bustamante, M. M. C., Opsahl, S., … Viana, L.
644   T.: Seasonal soil fluxes of carbon monoxide in burned and unburned Brazilian savannas, Journal of
645   Geophysical Research Atmospheres, 107(20), doi:10.1029/2001JD000638, 2002

646   Kuhlbusch, T. A., Zepp, R. G., Miller, W. L., & A BURKE, R.: Carbon monoxide fluxes of different soil
647   layers in upland Canadian boreal forests, Tellus B. Informa UK Limited, doi:10.1034/j.1600-
648   0889.1998.t01-3-00003.x, 1998

649   Lamarque, J. F., Emmons, L. K., Hess, P. G., Kinnison, D. E., Tilmes, S., Vitt, F., … Tyndall, G. K.: CAM-
650   chem: Description and evaluation of interactive atmospheric chemistry in the Community Earth System
651   Model, Geoscientific Model Development, 5(2), 369–411, https://doi.org/10.5194/gmd-5-369-2012, 2012

652   Lee, H., Rahn, T., & Throop, H.: An accounting of C-based trace gas release during abiotic plant litter
653   degradation, Global Change Biology, 18(3), 1185–1195, doi:10.1111/j.1365-2486.2011.02579.x, 2012

654   Logan, J. A., Prather, M. J., Wofsy, S. C., & McElroy, M. B.: Tropospheric chemistry - A global
655   perspective, J. Geophys. Res., doi:10.1029/JC086iC08p07210, 1981

656   Lu, Y., & Khalil, M. A. K.: Methane and carbon monoxide in OH chemistry: The effects of feedbacks and
657   reservoirs generated by the reactive products, Chemosphere. Elsevier BV, doi:10.1016/0045-
658   6535(93)90450-j, 1993

659   Luo, M., Read, W., Kulawik, S., Worden, J., Livesey, N., Bowman, K., & Herman, R.: Carbon monoxide
660   (CO) vertical profiles derived from joined TES and MLS measurements, Journal of Geophysical Research
661   Atmospheres, 118(18), 10601–10613, doi:10.1002/jgrd.50800, 2013

662   Moxley, J. M., & Smith, K. A.: Factors affecting utilisation of atmospheric CO by soils, Soil Biology and
663   Biochemistry, 30(1), 65–79, doi:10.1016/S0038-0717(97)00095-3, 1998

664   Myhre, G., Shindell, D., Bréon, F. M., Collins, W., Fuglestvedt, J., Huang, J., ... & Nakajima, T.:

665   Anthropogenic and Natural Radiative Forcing. In: Climate Change 2013: The Physical Science Basis,

666   Contribution of Working Group 1 to the Fifth Assessment Report of the Intergovernmental Panel on

667   Climate Change. Table, 8, 714, 2013

668   Nakai, T., Kim, Y., Busey, R. C., Suzuki, R., Nagai, S., Kobayashi, H., … Ito, A.: Characteristics of

669   evapotranspiration from a permafrost black spruce forest in interior Alaska. Polar Science, 7(2), 136–148.

670   doi:10.1016/j.polar.2013.03.003, 2013

671   Philip, R., & Novick, K.: AmeriFlux US-MMS Morgan Monroe State Forest [Data set]. AmeriFlux; Indiana

672   University, doi:10.17190/AMF/1246080, 2016

673   Pihlatie, M., Rannik, Ü., Haapanala, S., Peltola, O., Shurpali, N., Martikainen, P. J., … Mammarella, I.:

674   Seasonal and diurnal variation in CO fluxes from an agricultural bioenergy crop, Biogeosciences.

675   Copernicus GmbH, doi:10.5194/bg-13-5471-2016, 2016

676   Potter, C. S., Klooster, S. A., & Chatfield, R. B.: Consumption and production of carbon monoxide in soils:

677   A global model analysis of spatial and seasonal variation, Chemosphere, 33(6), 1175–1193,

678   doi:10.1016/0045-6535(96)00254-8, 1996

679   Prather, M., and Ehhalt, D.: Atmospheric chemistry and greenhouse gases. Climate Change, 2001: The

680   Scientific Basis (Houghton JT, Ding Y, Griggs DJ, Noguer M, van der Linden PJ, Dai X, Maskell K &

681   Johnson CA, eds), pp. 239–288, Cambridge University Press, Cambridge, UK, 2001

682   Prather, M., Derwent, R., Ehhalt, D., Fraser, P., Sanheeza, E. and Zhou, X.: Other trace gases and

683   atmospheric chemistry, Climate Change, 1994. Radiative Forcing of Climate Change (Houghton JT, Meira

684   Filho LG, Bruce J, Hoesung Lee BA, Callander E, Haites E, Harris N & Maskell K, eds), pp. 76–126,

685   Cambridge University Press, Cambridge, UK, 1995

686   SALESKA, S. R., DA ROCHA, H. R., HUETE, A. R., NOBRE, A. D., ARTAXO, P. E., & SHIMABUKURO,

687   Y. E.: LBA-ECO CD-32 Flux Tower Network Data Compilation, Brazilian Amazon: 1999-2006, ORNL

688   Distributed Active Archive Center, doi:10.3334/ORNLDAAC/1174, 2013

689   Sanderson, M. G., Collins, W. J., Derwent, R. G., & Johnson, C. E.: Simulation of global hydrogen levels

690   using a Lagrangian three-dimensional model, Journal of Atmospheric Chemistry, 46(1), 15–28,

691   doi:10.1023/A:1024824223232, 2003

692   Sanhueza, E., Dong, Y., Scharffe, D., Lobert, J. M., & Crutzen, P. J.: Carbon monoxide uptake by

693   temperate forest soils: The effects of leaves and humus layers, Tellus, Series B: Chemical and Physical

694   Meteorology, 50(1), 51–58, doi:10.1034/j.1600-0889.1998.00004.x, 1998

695   Schade, G. W., & Crutzen, P. J.: CO emissions from degrading plant matter (II). Estimate of a global

696   source strength, Tellus, Series B: Chemical and Physical Meteorology, 51(5), 909–918,

697   doi:10.1034/j.1600-0889.1999.t01-4-00004.x, 1999

698   Scharffe, D., Hao, W. M., Donoso, L., Crutzen, P. J., & Sanhueza, E.: Soil fluxes and atmospheric

699   concentration of CO and CH4 in the northern part of the Guayana shield, Venezuela, Journal of

700   Geophysical Research-Atmospheres, 95(90), 22475–22480, doi:10.1029/JD095iD13p22475, 1990

Seiler, W.: In: Krumbein, W.E. (Ed.), Environmental Biogeochemistry and Geomicrobiology, Methods, Metals and Assessment, vol. 3, Ann Arbor Science, Ann Arbor, MI, pp. 773-810, 1987

Seinfeld, J. H., & Pandis, S. N.: Atmospheric Chemistry and Physics: From Air Pollution to Climate Change, Atmospheric Chemistry and Physics from Air Pollution to Climate Change Publisher New York NY Wiley 1998 Physical Description Xxvii 1326 p A WileyInterscience Publication ISBN 0471178152, 51, 1–4, doi:10.1080/00139157.1999.10544295, 1998

Stein, O., Schultz, M. G., Bouarar, I., Clark, H., Huijnen, V., Gaudel, A., … Clerbaux, C.: On the wintertime low bias of Northern Hemisphere carbon monoxide found in global model simulations, Atmospheric Chemistry and Physics, 14(17), 9295–9316, doi:10.5194/acp-14-9295-2014, 2014

Stevenson, D. S., Dentener, F. J., Schultz, M. G., Ellingsen, K., van Noije, T. P. C., Wild, O., … Szopa, S.: Multimodel ensemble simulations of present-day and near-future tropospheric ozone, Journal of Geophysical Research Atmospheres, 111(8), doi:10.1029/2005JD006338, 2006

Suzuki, R.: AmeriFlux US-Prr Poker Flat Research Range Black Spruce Forest [Data set], AmeriFlux; Japan Agency for Marine-Earth Science and Technology, doi:10.17190/AMF/1246153, 2016

Tan, Z., & Zhuang, Q.: An analysis of atmospheric CH4 concentrations from 1984 to 2008 with a single box atmospheric chemistry model, Atmospheric Chemistry and Physics Discussions, Copernicus GmbH, doi:10.5194/acpd-12-30259-2012, 2012

Tarr, M. a., Miller, W. L., & Zepp, R. G.: Direct carbon monoxide photoproduction from plant matter, Journal of Geophysical Research, 100, 11403, doi:10.1029/94JD03324, 1995

Taylor, J. A., Zimmerman, P. R., & Erickson, D. J.: A 3-D modelling study of the sources and sinks of atmospheric carbon monoxide, Ecological Modelling, 88(1–3), 53–71, doi:10.1016/0304-3800(95)00069-0, 1996

van Asperen, H., Warneke, T., Sabbatini, S., Nicolini, G., Papale, D., & Notholt, J.: The role of photo- and thermal degradation for CO₂ and CO fluxes in an arid ecosystem, Biogeosciences, 12(13), 4161–4174, doi:10.5194/bg-12-4161-2015, 2015

Varella, R. F., Bustamante, M. M. C., Pinto, A. S., Kisselle, K. W., Santos, R. V., Burke, R. A., … Viana, L. T.: Soil fluxes of CO2, CO, NO, and N2O from an old pasture and from native Savanna in Brazil, Ecological Applications, 14(4 SUPPL.), doi:10.1890/01-6014, 2004

Vreman, H. J., Wong, R. J., & Stevenson, D. K.: Quantitating carbon monoxide production from heme by vascular plant preparations in vitro, Plant Physiology and Biochemistry, 49(1), 61–68, doi:10.1016/j.plaphy.2010.09.021, 2011

Wesely, M. L.: Parameterization of surface resistances to gaseous dry deposition in regional-scale numerical models. Atmospheric Environment (1967), Elsevier BV, doi:10.1016/0004-6981(89)90153-4, 1989

Wesely, M., & Hicks, B.: A review of the current status of knowledge on dry deposition. Atmospheric Environment, 34, 2261–2282, doi:10.1016/S1352-2310(99)00467-7, 2000

738 Whalen, S. C., & Reeburgh, W. S.: Carbon monoxide consumption in upland boreal forest soils, Soil
739 Biology and Biochemistry, 33(10), 1329–1338, doi:10.1016/S0038-0717(01)00038-4, 2001

740 Yonemura, S., Kawashima, S., & Tsuruta, H.: Carbon monoxide, hydrogen, and methane uptake by soils
741 in a temperate arable field and a forest, Journal of Geophysical Research, 105(Dll), 14347,
742 https://doi.org/10.1029/1999JD901156, 2000

743 Yoon, J., & Pozzer, A.: Model-simulated trend of surface carbon monoxide for the 2001-2010
744 decade, Atmospheric Chemistry and Physics, 14(19), 10465–10482, doi:10.5194/acp-14-10465-2014,
745 2014

746 Zepp, R. G., Miller, W. L., Tarr, M. A., Burke, R. A., & Stocks, B. J.: Soil-atmosphere fluxes of carbon
747 monoxide during early stages of postfire succession in upland Canadian boreal forests, Journal of
748 Geophysical Research-Atmospheres, 102(D24), 29301–29311, doi:10.1029/97jd01326, 1997

749 Zhuang, Q., McGuire, A. D., Melillo, J. M., Clein, J. S., Dargaville, R. J., Kicklighter, D. W., … Hobbie, J.
750 E.: Carbon cycling in extratropical terrestrial ecosystems of the Northern Hemisphere during the 20th
751 century: A modeling analysis of the influences of soil thermal dynamics, Tellus, Series B: Chemical and
752 Physical Meteorology, 55(3), 751–776, doi:10.1034/j.1600-0889.2003.00060.x, 2003

753 Zhuang, Q., Melillo, J. M., Kicklighter, D. W., Prinn, R. G., McGuire, A. D., Steudler, P. A., … Hu, S.:
754 Methane fluxes between terrestrial ecosystems and the atmosphere at northern high latitudes during the
755 past century: A retrospective analysis with a process-based biogeochemistry model, Global
756 Biogeochemical Cycles, 18(3), doi:10.1029/2004GB002239, 2004

757 Zhuang, Q., Melillo, J. M., McGuire, A. D., Kicklighter, D. W., Prinn, R. G., Steudler, P. A., … Hu, S.: Net
758 emissions of CH4 and CO2 in Alaska: Implications for the region's greenhouse gas budget, Ecological
759 Applications, 17(1), 203–212, doi:10.1890/1051-0761(2007)017[0203:NEOCAC]2.0.CO;2, 2007

760 Zhuang, Q., Romanovsky, V. E., & McGuire, a. D.: Incorporation of a permafrost model into a large-scale
761 ecosystem model: Evaluation of temporal and spatial scaling issues in simulating soil thermal
762 dynamics, Journal of Geophysical Research, 106, 33649, doi:10.1029/2001JD900151, 2001

763 Zhuang, Q., Chen, M., Xu, K., Tang, J., Saikawa, E., Lu, Y., … McGuire, A. D.: Response of global soil
764 consumption of atmospheric methane to changes in atmospheric climate and nitrogen deposition, Global
765 Biogeochemical Cycles, doi:10.1002/gbc.20057, 2013

Table 1. Model parameterization sites for thermal and hydrology modules (site No. 1-4) and for CODM module (site No. 5-13)

No.	Site Name	Location	Vegetation	Driving Climate	Observed Data	Source and Comments
1	Poker Flat Research Range Black Spruce Forest (US_PRR)	147°29'W/65°7'N	Boreal Evergreen Needle Leaf Forests	Site Observation & ERA Interim	Soil Temperature and Moisutre of 2011-2014	Suzuki (2016)
2	Morgan Monroe State Forest (US_MMS)	86°25'W/39°19'N	Temperate Deciduous Broadleaf Forests	Site Observation & ERA Interim	Soil Temperature and Moisutre of 1999-2014	Philip and Novick (2016)
3	Santarem, Tapajos National Forest (STM_K83)	54°56'W/3°3'S	Tropical Moist Forest	Site Observation & ERA Interim	Soil Temperature and Moisutre of 2000-2004	SALESKA et al. (2013)
4	Bananal Island Site (TOC_BAN)	50°08'W/9°49'S	Tropical Forest-Savanna	Site Observation & ERA Interim	Soil Temperature and Moisutre of 2003-2006	SALESKA et al. (2013)
5	Eastern Finland (EF)	27°14E/63°9'N	Boreal Grassland	Site Observation & ERA Interim	CO flux of April-November,2011	Pihlatie et.al. (2016)
6	Viterbo, Italy (VI)	11°55'E/42°22'N	Mediterranean Grassland	Site Observation & ERA Interim	CO flux of August, 2013	van Asperen et al. (2015)
7	Brasilia, Brazil (BB)	47°51'W/15°56'S	Tropical Savanna	Site Observation & CRU	CO flux of October 1999 to July 2001	Varella et al. (2004)
8	Orange County, North Carolina (OC)	79°7'W/35°58'N	Temperate Coniferous Forest	AMF_US-Dk3 2002-2003	CO flux of March 2002 to March 2003	Fisher (2003)
9	Tsukuba Science City, Japan (TSC)	140°7'E/36°01'N	Temperate Mixed Forest	Site Observation & ERA Interim	CO flux of July 1996 to September 1997	Yonemura et. al. (2000)
10	Manitoba, Canada (CBS)	96°44'W/56°09'N	Boreal Pine Forest	Site Observation & AMF_CA-Man	CO flux of June-August, 1994	Kuhlbusch et. al (1998)
11	Scotland, U.K. (SUK)	3°12'W/55°51'N	Temperate Deciduous Forests	ERA Interim 1995	CO flux of 1995	Moxley and Smith (1998)
12	Alaska, USA (AUS)	147°41'W/64°52'N	Boreal wetland	CRU 1991	CO flux of Lab Experiment,1991	Funk et al. (1994)
13	Guayana Shield,Bolivar State,Venezuela (GBV)	62°57'W/7°51'N	Tropical Smideciduous Forest	CRU 1985	CO flux of Lab Experiment,1985	Scharffe et al. (1990)

Table 2. Ecosystem-specific parameters in the CODM module[a]

	Ecosystem Type	k_{CO} (ul CO l⁻¹ g⁻¹ h⁻¹)	V_{max} (ug CO g⁻¹ h⁻¹)	T_{ref} (°C)	$Q10$ (Unitless)	M_{min} ($\frac{v}{v}$)	M_{max} ($\frac{v}{v}$)	M_{opt} ($\frac{v}{v}$)	E_{soc}	F_{soc} ($\frac{g}{g}$)	$\frac{Ea_{ref}}{R}$ (K)	PM_{ref} ($\frac{v}{v}$)	PT_{ref} (°C)
1	Alpine Tundra & Polar Desert	36.00	0.78	4.00	1.80	0.10	1.00	0.55	3.00	0.33	7700	0.25	30.00
2	Wet Tundra	36.00	0.70	4.00	1.80	0.25	1.00	0.55	3.00	0.42	7700	0.25	30.00
3	Boreal Forest	27.34	1.18	9.81	1.60	0.15	0.64	0.53	2.98	0.50	8827	0.35	26.99
4	Temperate Coniferous Forest	42.64	2.15	6.90	1.87	0.02	0.96	0.53	2.86	0.50	8404	0.38	31.52
5	Temperate Deciduous Forest	40.16	2.43	8.54	1.51	0.17	0.81	0.51	2.45	0.50	8801	0.35	37.44
6	Grassland	42.41	0.49	11.27	1.65	0.16	0.82	0.51	3.09	0.42	14165	0.24	12.29
7	Xeric Shrublands	8.00	0.30	4.00	1.50	0.10	1.00	0.55	3.00	0.33	7700	0.25	30.00
8	Tropical Forest	45.00	2.00	4.00	1.50	0.10	1.00	0.55	3.80	0.50	14000	0.50	18.00
9	Xeric Woodland	8.00	0.30	4.00	1.50	0.10	1.00	0.55	3.00	0.50	7700	0.25	30.00
10	Temperate Evergreen Broadleaf Forest	40.16	2.43	8.54	1.51	0.17	0.81	0.51	2.45	0.50	8801	0.35	37.44
11	Mediterranean Shrubland	45.00	1.50	4.00	1.50	0.10	1.00	0.55	3.00	0.33	7700	0.25	30.00
**	Largest Potential Value	51.00	11.1	15.00	2.00	0.30	1.00	0.60	3.80	--	15000	0.60	40.00

[a] k_{CO} is the half-saturation constant for soil CO concentration; V_{max} is the specific maximum CO oxidation rate; T_{ref} is the reference temperature to account for soil temperature effects on CO consumption; $Q10$ is the an ecosystem-specific Q10 coefficient to account for soil temperature effects on CO consumption; M_{min}, M_{max}, M_{opt} are the minimum, optimum, and maximum volumetric soil moistures of oxidation reaction to account for soil moisture effects on CO consumption; E_{soc} is an estimated nominal CO production factor, similar as Potter et al. (1996) (10⁻⁴ mg CO m⁻² d⁻¹ per g SOC m⁻²); F_{soc} is a constant fraction of top 20cm SOC compared to total amount of SOC to account for SOC effects on CO production; Ea_{ref}/R is the is the ecosystem-specific activation energy divided by gas constant to account for the reaction rate of production; PM_{ref} is the reference moisture to account for soil temperature effects on CO production; PT_{ref} is the reference temperature to account for soil temperature effects on CO production

772   **Table 3.** Regional soil CO consumption, net flux and production (Tg CO yr^{-1}) during 2000-2013

	South-45S	45S-0	0-45N	45N-North	Global
Consumption	0.22	75.77	91.66	18.90	186.55
Net flux	0.13	59.34	77.17	14.63	151.27
Production	0.09	16.43	14.49	4.27	35.28

773

774

Table 4. Annual total soil CO consumption, net flux and production in different ecosystems during 2000-2013 (E1) and mean CO deposition velocity in different ecosystems during 1901-2013 (E2)

Vegetation Type	Area (10^6 km^2)	Pixels	Consumption (Tg CO yr^{-1})	Net flux (Tg CO yr^{-1})	Production (Tg CO yr^{-1})	Deposition velocity (mm s^{-1})
Alpine Tundra & Polar Desert	5.28	3580	-0.92	-0.69	0.23	0.023
Wet Tundra	5.24	4212	-1.00	-0.42	0.58	0.015
Boreal Forest	12.47	7578	-7.76	-6.01	1.75	0.070
Forested Boreal Wetland	0.23	130	-0.14	-0.09	0.04	0.109
Boreal Woodland	6.48	4545	-2.48	-1.54	0.94	0.036
Non-Forested Boreal Wetland	0.83	623	-0.35	-0.18	0.17	0.029
Mixed Temperate Forest	5.25	2320	-10.49	-9.98	0.51	0.204
Temperate Coniferous Forest	2.49	1127	-3.51	-3.21	0.30	0.185
Temperate Deciduous Forests	3.65	1666	-5.07	-4.83	0.25	0.151
Temperate Forested Wetland	0.15	60	-0.35	-0.35	0.01	0.281
Tall Grassland	3.63	1567	-1.66	-0.65	1.01	0.021
Short Grassland	4.71	2072	-1.05	-0.27	0.78	0.010
Tropical Savanna	13.85	4666	-21.86	-15.88	5.98	0.234
Xeric Shrubland	14.71	5784	-1.95	-1.64	0.31	0.021
Tropical Evergreen Forest	17.77	5855	-85.90	-69.66	16.24	0.879
Tropical Forested Wetland	0.55	178	-3.59	-3.09	0.50	1.154
Tropical Deciduous Forest	4.69	1606	-14.81	-11.78	3.03	0.532
Xeric Woodland	6.85	2387	-8.48	-7.44	1.04	0.246
Tropical Forested Floodplain	0.15	50	-0.89	-0.77	0.12	1.117
Desert	11.61	4170	-0.62	-0.57	0.05	0.008
Tropical Non-forested Wetland	0.06	19	-0.03	-0.02	0.01	0.067
Tropical Non-forested Floodplain	0.36	120	-0.35	-0.24	0.10	0.083
Temperate Non-Forested Weland	0.34	120	-0.33	-0.20	0.14	0.089
Temperate Forested Floodplain	0.10	48	-0.13	-0.12	0.00	0.197
Temperate Non-forested Floodplain	0.10	45	-0.05	-0.03	0.02	0.050
Wet Savanna	0.16	59	-0.39	-0.32	0.07	0.434
Salt Marsh	0.09	35	-0.05	-0.03	0.03	0.035
Mangroves	0.12	38	-0.49	-0.41	0.08	0.809
Temperate Savannas	6.83	2921	-3.83	-3.22	0.61	0.076
Temperate Evergreen Broadleaf	3.33	1268	-7.17	-6.95	0.22	0.252
Mediterranean Shrubland	1.47	575	-0.86	-0.71	0.16	0.100
Total	133.56	59424	-186.55	-151.27	35.28	--

782

Table 5. Sensitivity of global CO consumption, net flux and production (Tg CO yr^{-1}) to changes in atmospheric

CO, soil organic carbon (SOC), precipitation (Prec) and air temperature (AT)

	Baseline	CO +30%	CO -30%	SOC +5%	SOC -5%	Prec +30%	Prec -30%	AT +3°C	AT -3°C
Consumption	-147.65	-164.14	-131.12	-152.27	-143.03	-150.72	-143.50	-190.59	-114.83
Change (%)	0.00	11.17	-11.19	3.13	-3.13	2.08	-2.81	29.09	-22.23
Net flux	-113.65	-130.15	-97.12	-116.58	-110.73	-116.97	-109.32	-144.23	-89.58
Change (%)	0.00	14.51	-14.54	2.57	-2.57	2.92	-3.81	26.90	-21.18
Production	33.99	33.99	33.99	35.69	32.29	33.74	34.17	46.36	25.25
Change (%)	0.00	0.00	0.00	5.00	-5.00	-0.75	0.53	36.39	-25.72

785

786

787

788

789

790

791

792

793

794

795

796

797

798

799

800

801

802

803

Table 6. Correlation coefficients between forcing variables (precipitation (Prec), air temperature (Tair), soil organic carbon (SOC), soil temperature (Tsoil), soil moisture (Msoil) and atmospheric CO (CO air)) and absolute values of consumption, production and net flux for different regions and the globe

		Monthly					Annual				
		North-45°N	45°N-0°	0°-45°S	45°S-South	Global	North-45°N	45°N-0°	0°-45°S	45°S-South	Global
Prec	Consumption	0.91	0.96	0.92	-0.34	0.87	0.65	0.21	0.26	0.13	0.52
	Production	0.91	0.70	0.45	-0.34	0.82	0.63	0.10	0.15	-0.11	0.47
	Net flux	0.91	0.97	0.94	-0.33	0.87	0.65	0.25	0.31	0.32	0.54
Tair	Consumption	0.97	0.98	0.91	0.96	0.95	0.92	0.93	0.88	0.84	0.91
	Production	0.96	0.83	0.72	0.98	0.94	0.92	0.92	0.91	0.95	0.91
	Net Flux	0.97	0.97	0.88	0.90	0.95	0.91	0.92	0.85	0.62	0.91
SOC	Consumption	-0.19	0.07	0.21	-0.01	0.15	0.68	0.90	0.92	0.47	0.92
	Production	-0.19	0.31	0.47	-0.02	0.24	0.72	0.92	0.92	0.50	0.93
	Net Flux	-0.19	0.03	0.14	0.00	0.13	0.67	0.88	0.91	0.38	0.91
Tsoil	Consumption	0.97	0.98	0.92	0.96	0.95	0.94	0.93	0.88	0.85	0.95
	Production	0.97	0.83	0.72	0.98	0.94	0.94	0.92	0.91	0.96	0.95
	Net Flux	0.98	0.97	0.88	0.90	0.95	0.93	0.93	0.86	0.63	0.95
Msoil	Consumption	0.85	0.96	0.92	0.19	0.76	0.03	0.22	0.14	0.26	0.22
	Production	0.85	0.75	0.44	0.14	0.69	-0.02	0.12	0.02	0.05	0.17
	Net Flux	0.84	0.96	0.95	0.25	0.77	0.04	0.26	0.19	0.40	0.24
CO Air	Consumption	-0.66	-0.76	-0.29	0.14	-0.48	0.87	0.88	0.81	0.98	0.91
	Production	-0.70	-0.66	0.08	-0.40	-0.66	-0.36	-0.48	-0.54	-0.44	-0.57
	Net Flux	-0.64	-0.73	-0.35	0.55	-0.41	0.92	0.91	0.88	0.99	0.94

818
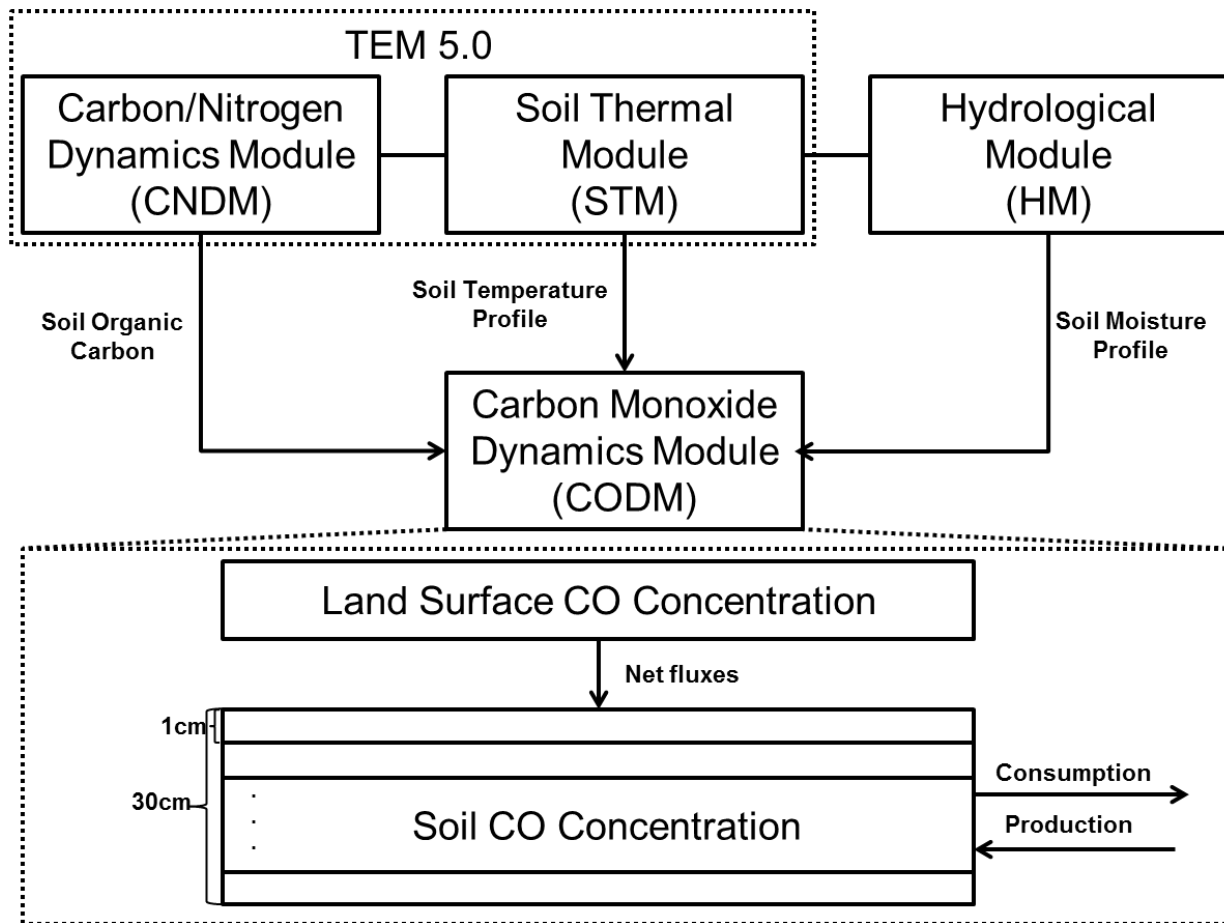
819   **Figure 1. The model framework** includes a carbon and nitrogen dynamics module (CNDM), a soil thermal module (STM)

820   from Terrestrial Ecosystem Model (TEM) 5.0 (Zhuang et al., 2001, 2003), a hydrological module (HM) based on a Land

821   Surface Module (Bonan, 1996; Zhuang et al., 2004), and a carbon monoxide dynamics module (CODM). The detailed

822   structure of CODM includes land surface CO concentration as top boundary and thirty 1 cm thick layers (totally 30 cm)

823   where consumption and production take place.

824

825

826

827

828
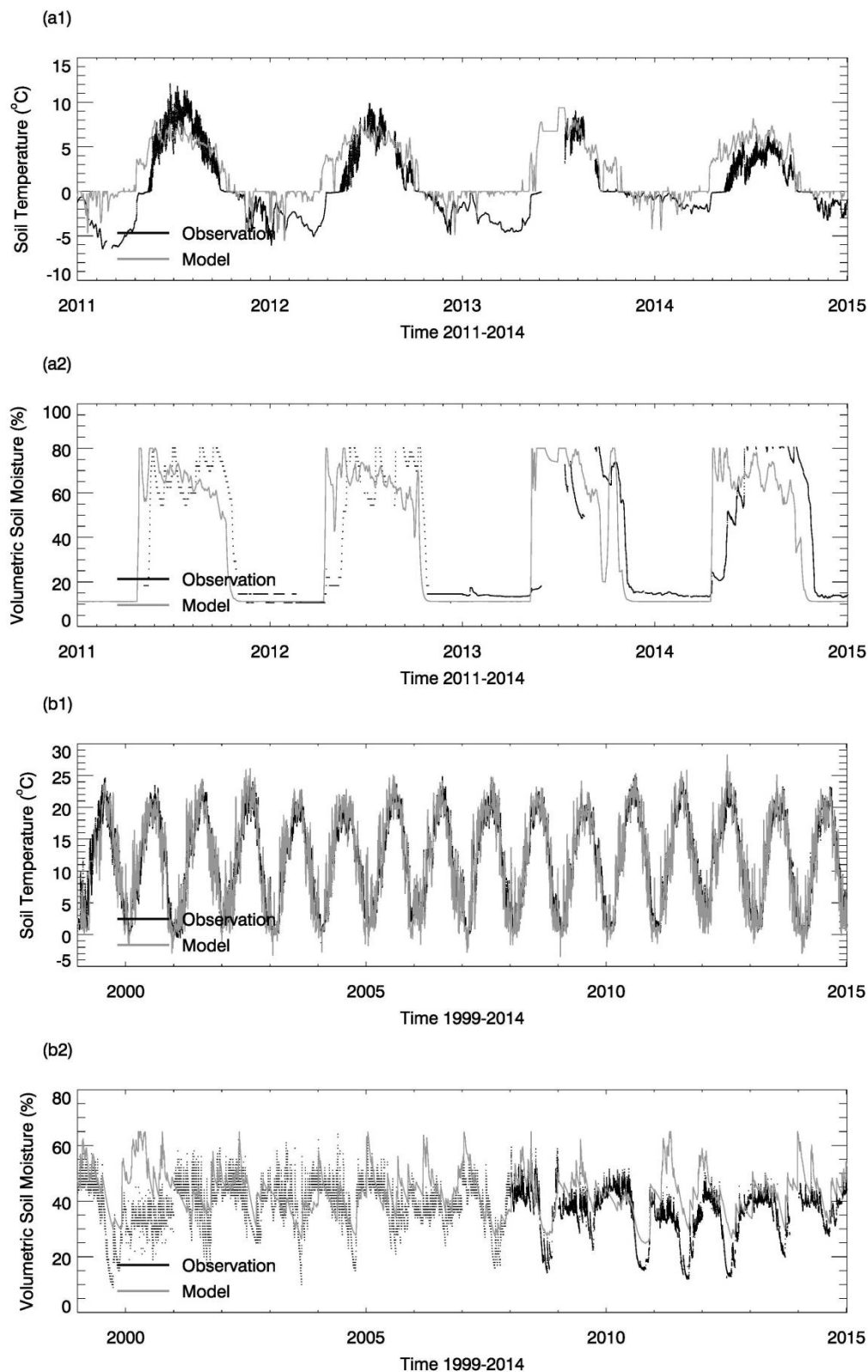
Figure 2. Evaluation of thermal and hydrology module at four sites: (a) Boreal Evergreen Needle Leaf Forests, (b) Temperate Deciduous Broadleaf Forests. (1) shows the soil temperature comparison between model simulations (gray line) and observations (black line) and (2) shows the soil moisture comparison between model simulations (gray line) and observations (black line). Specifically, the volumetric soil moisture is converted from the water content reflectometry (WCR) probe output period using an empirical calibration function of Bourgeau-Chavez et al. (2012) for 5cm-30cm layer. Some of them resulted in calculations of values greater than 100% VSM in Nakai et al. (2013) study. Our model estimated high VSM (close to 80%) is due to top 10 cm moss in the model which has a saturation VSM of 0.8
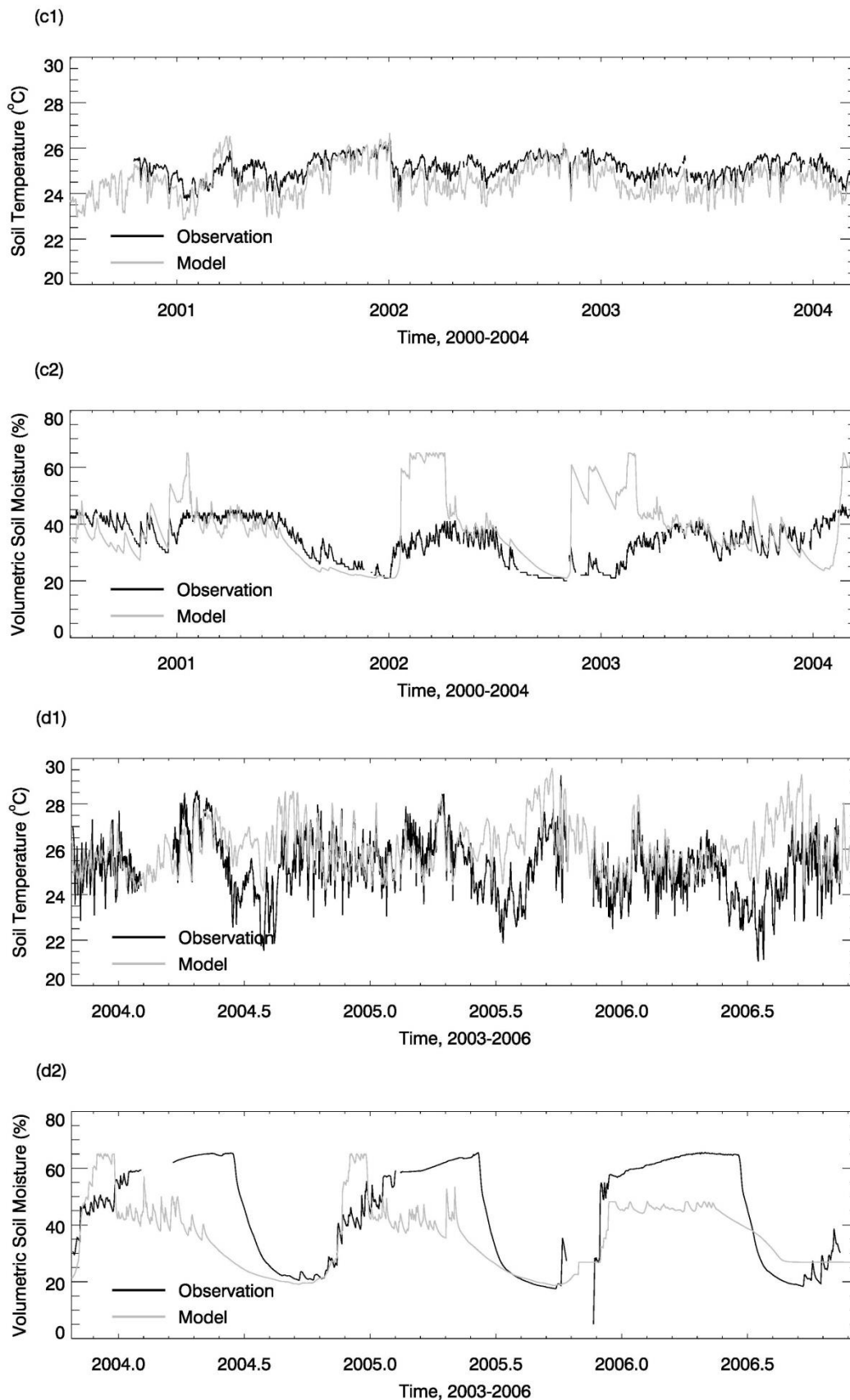
Figure 2. Contd. Evaluation of thermal and hydrology module at four sites: (c) Tropical Moist Forest, (d) Tropical Forest-Savanna. (1) shows the soil temperature comparison between model simulations (gray line) and observations (black line) and (2) shows the soil moisture comparison between model simulations (gray line) and observations (black line)
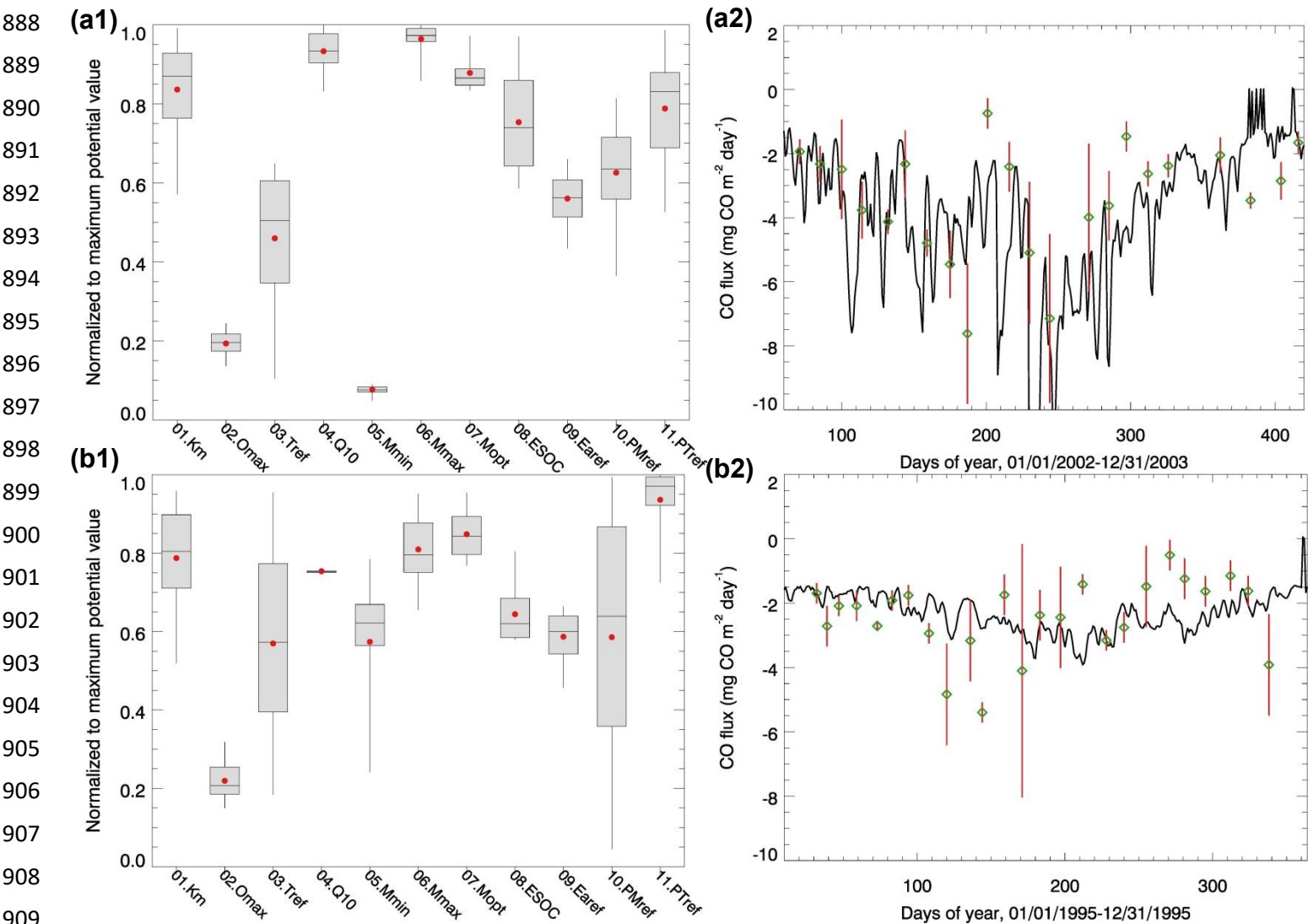
Figure 3. Parameter ensemble experiment results: Each parameter has 50 calibrated values generated from running SCE-UA-R 50 times independently. Parameters are normalized to their largest potential values described in Table 2. (a1) and (a2) are temperate coniferous forest normalized parameter distribution boxplots and CO flux comparisons between model simulations (solid line, using mean value of parameters) and observations (green diamond, red lines represent error bar, site No.8), respectively. For each box, line top, box top, horizontal line inside box, box bottom and line bottom represent maximum, third quartile, median, first quartile and minimum of 50 parameter values. Red dot represents the mean value of 50 parameter values. (b1) and (b2) are plots for temperate deciduous forest (site No.11).
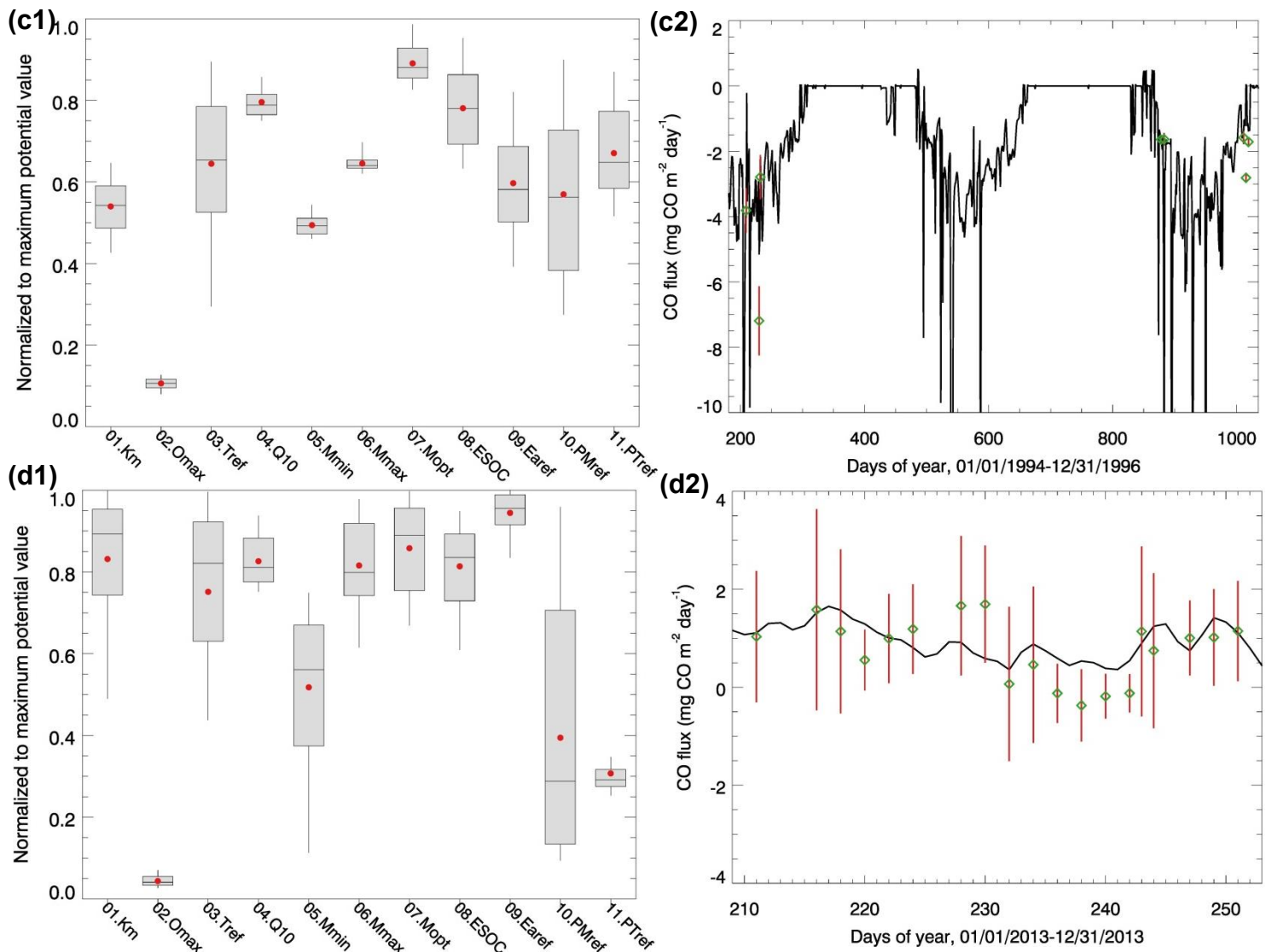
Figure 3. Contd. Parameter ensemble experiment results: Each parameter has 50 calibrated values generated from running SCE-UA-R 50 times independently. Parameters are normalized to their largest potential values described in Table 2. (c1) and (c2) are boreal forest normalized parameter distribution boxplots and CO flux comparisons between model simulations (solid line, using mean value of parameters) and observations (green diamond, red lines represent error bar, site No. 12), respectively. For each box, line top, box top, horizontal line inside box, box bottom and line bottom represent maximum, third quartile, median, first quartile and minimum of 50 parameter values. Red dot represents the mean value of 50 parameter values. (d1) and (d2) are for grassland (site No.6). Grassland observation data is the sum of hourly observations so error bar represented the standard deviation.

944
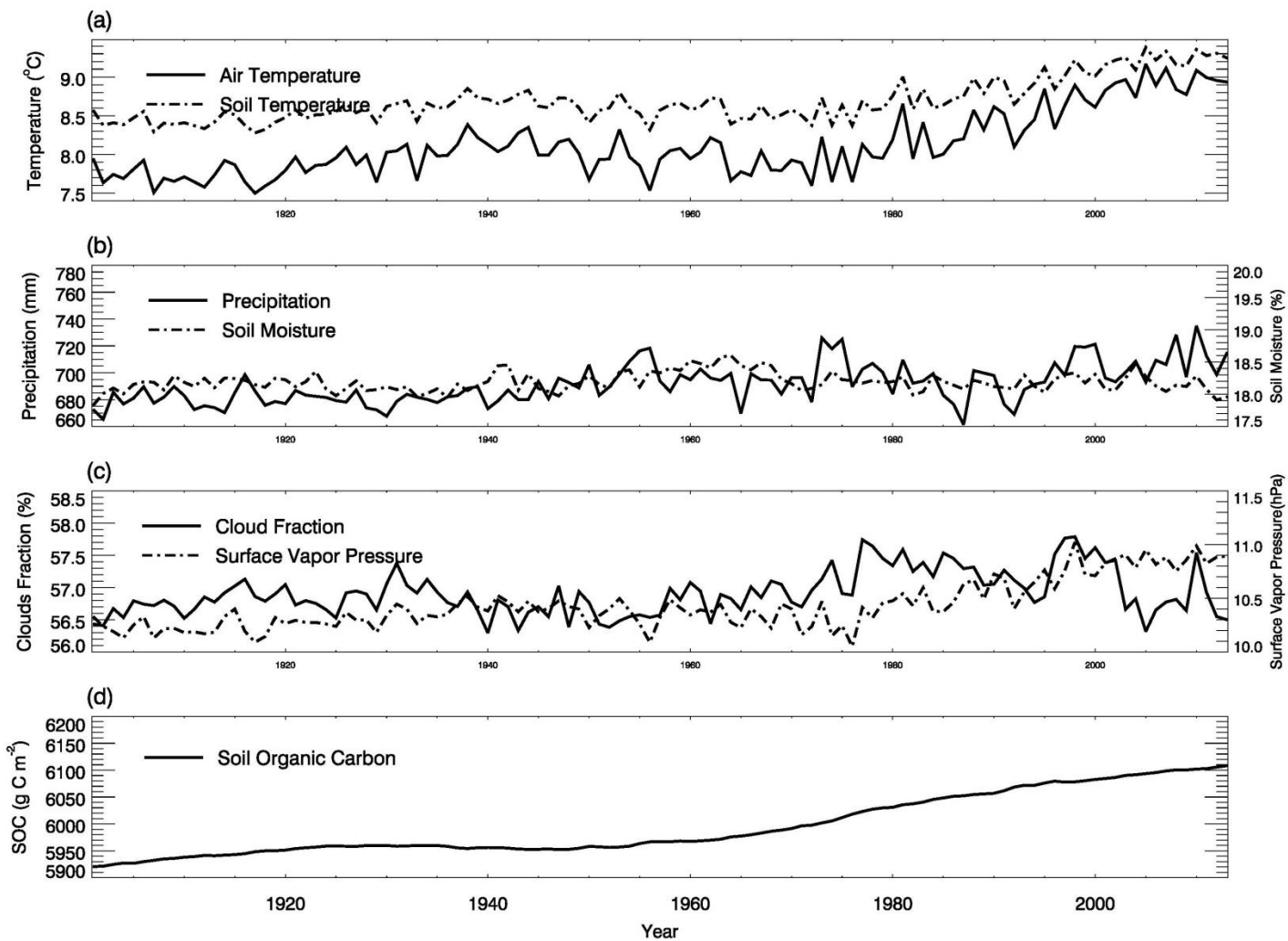
Figure 4. Historical global land surface (excluding Antarctic area and ocean area) mean climate, and simulated global mean soil moisture, soil temperature and SOC for the period 1901-2013.

947

948
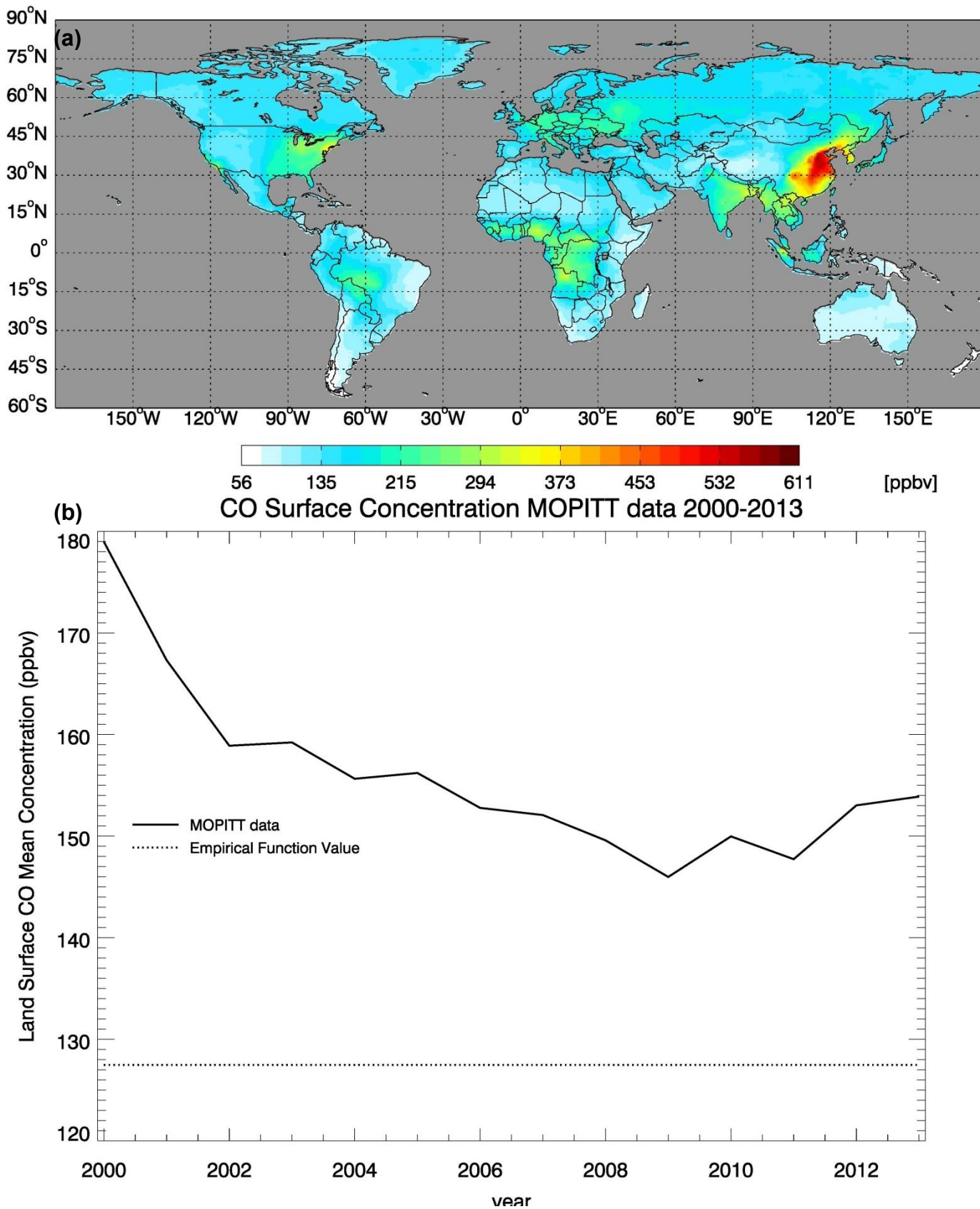
Figure 5. CO surface concentration data from MOPITT satellite (ppbv): (a) global mean CO surface concentrations from MOPITT during 2000-2013; (b) the CO annual surface concentrations from both MOPITT and empirical functions (Potter et al., 1996).
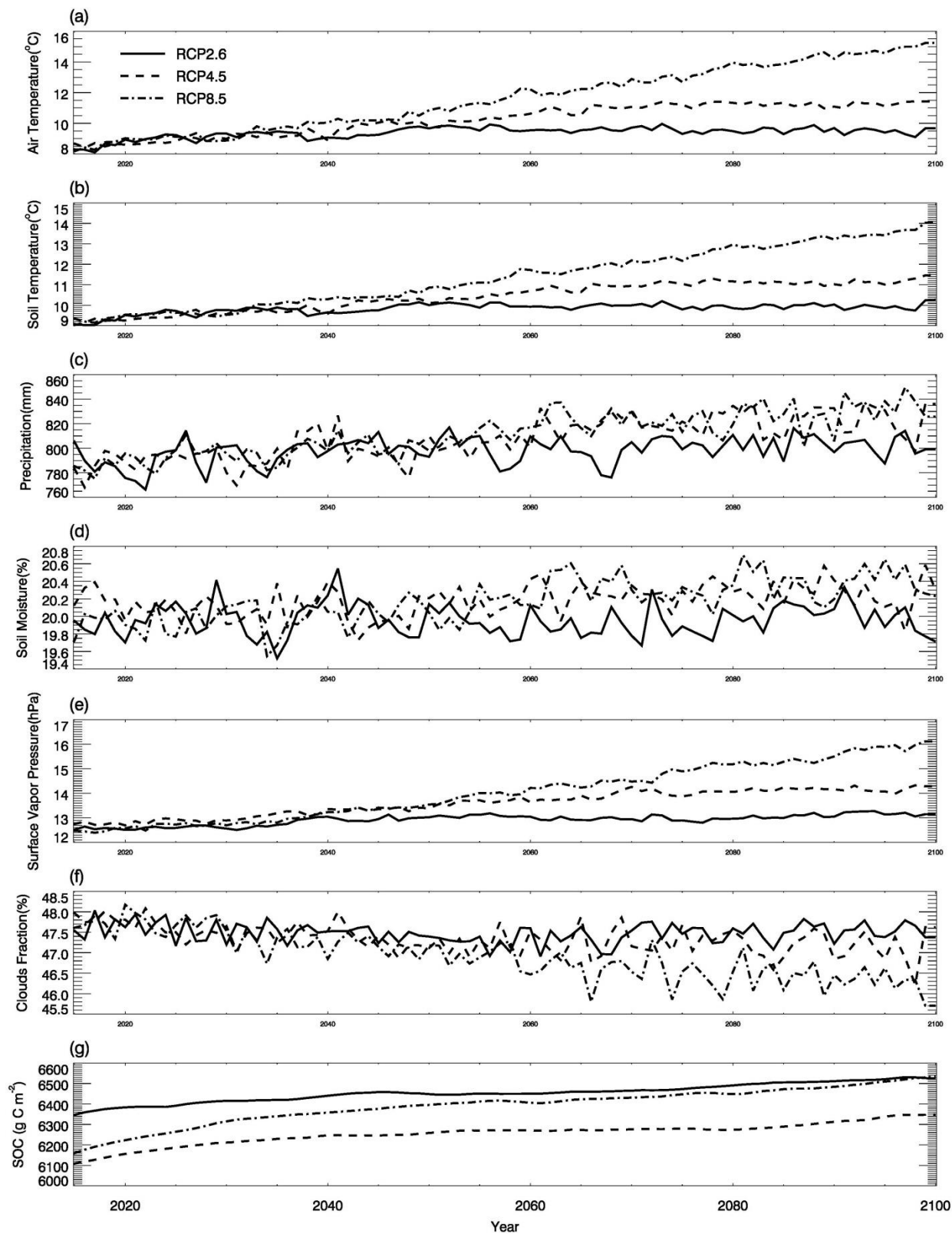
Figure 6. Global land surface (excluding Antarctic area and ocean area) mean climate from RCP2.6, RCP4.5 and RCP8.5 data sets and simulated mean soil temperature, moisture and SOC: (a)-(g) are land surface air temperature (°C), soil temperature (°C), precipitation (mm), soil moisture (%), surface water vapor pressure (hpa), cloud fraction (%), and SOC (mg m^{-2}), respectively.
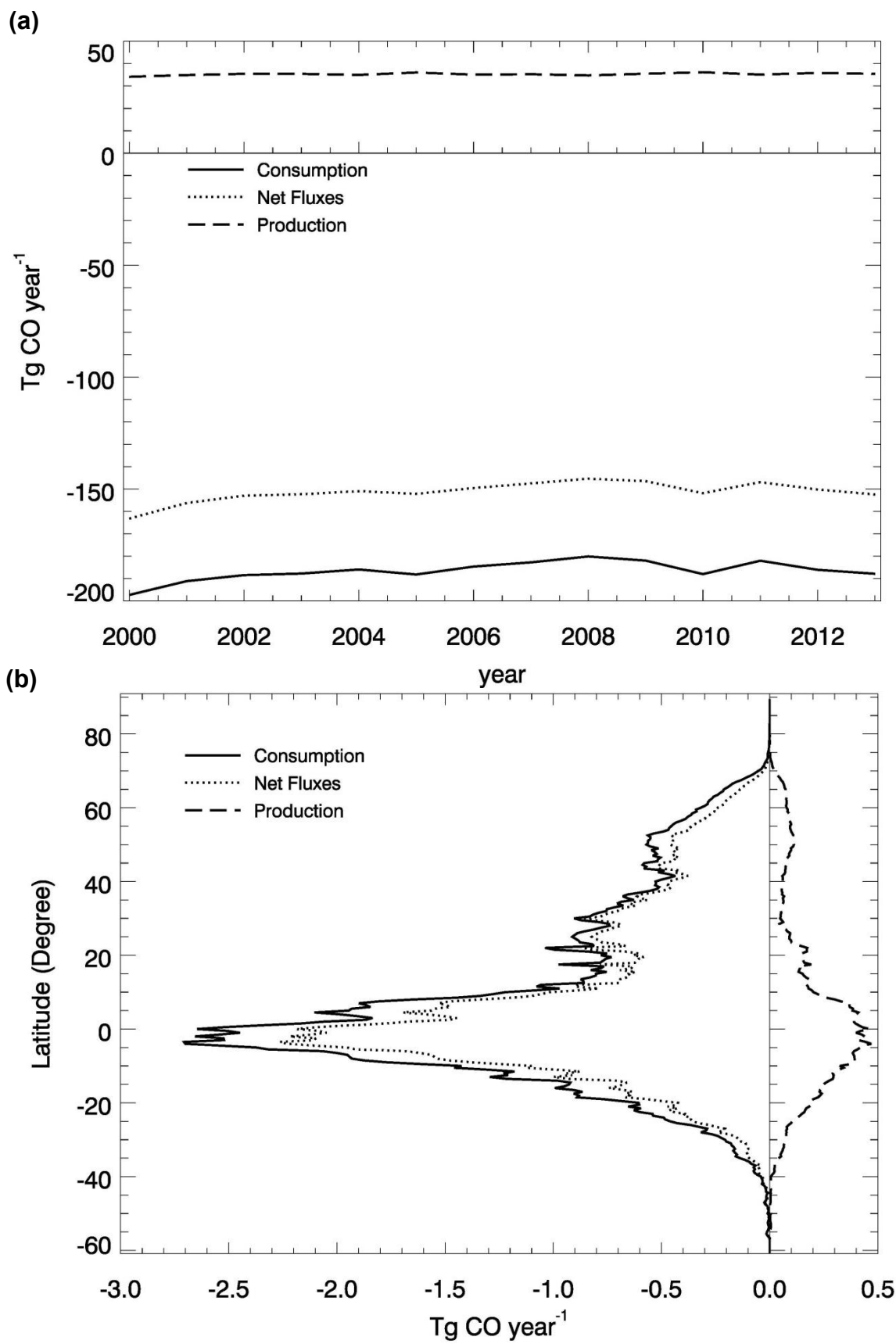
Figure 7. Global mean soil CO consumption, production and net flux: (a) annual time series during 2000-2013and (b) latitudinal distribution during 2000-2013.

035

036
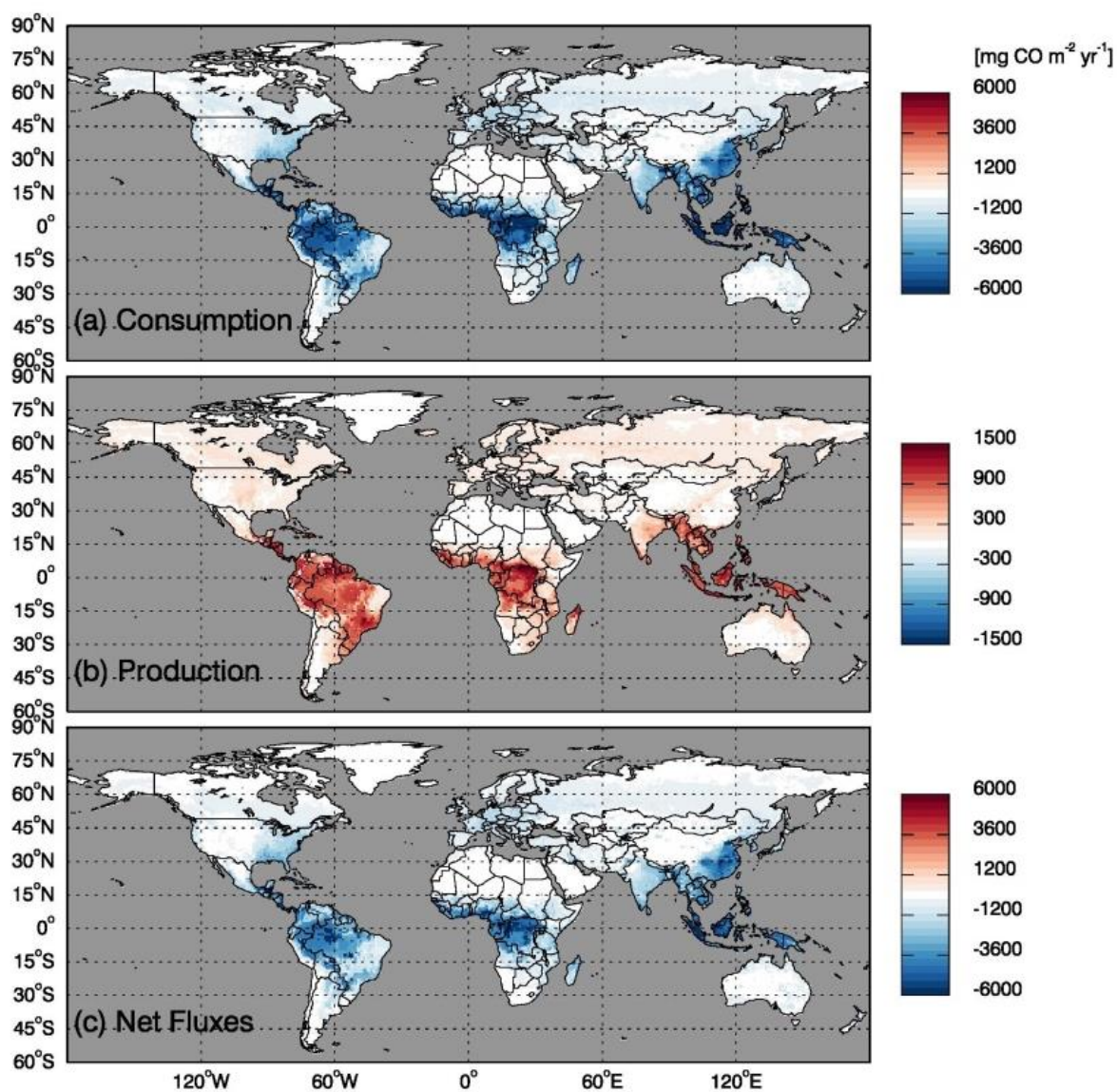
Figure 8. Global annual mean soil CO fluxes (mg CO m^{-2} yr^{-1}) during 2000-2013 using MOPITT CO atmospheric surface concentration data (right side)

037
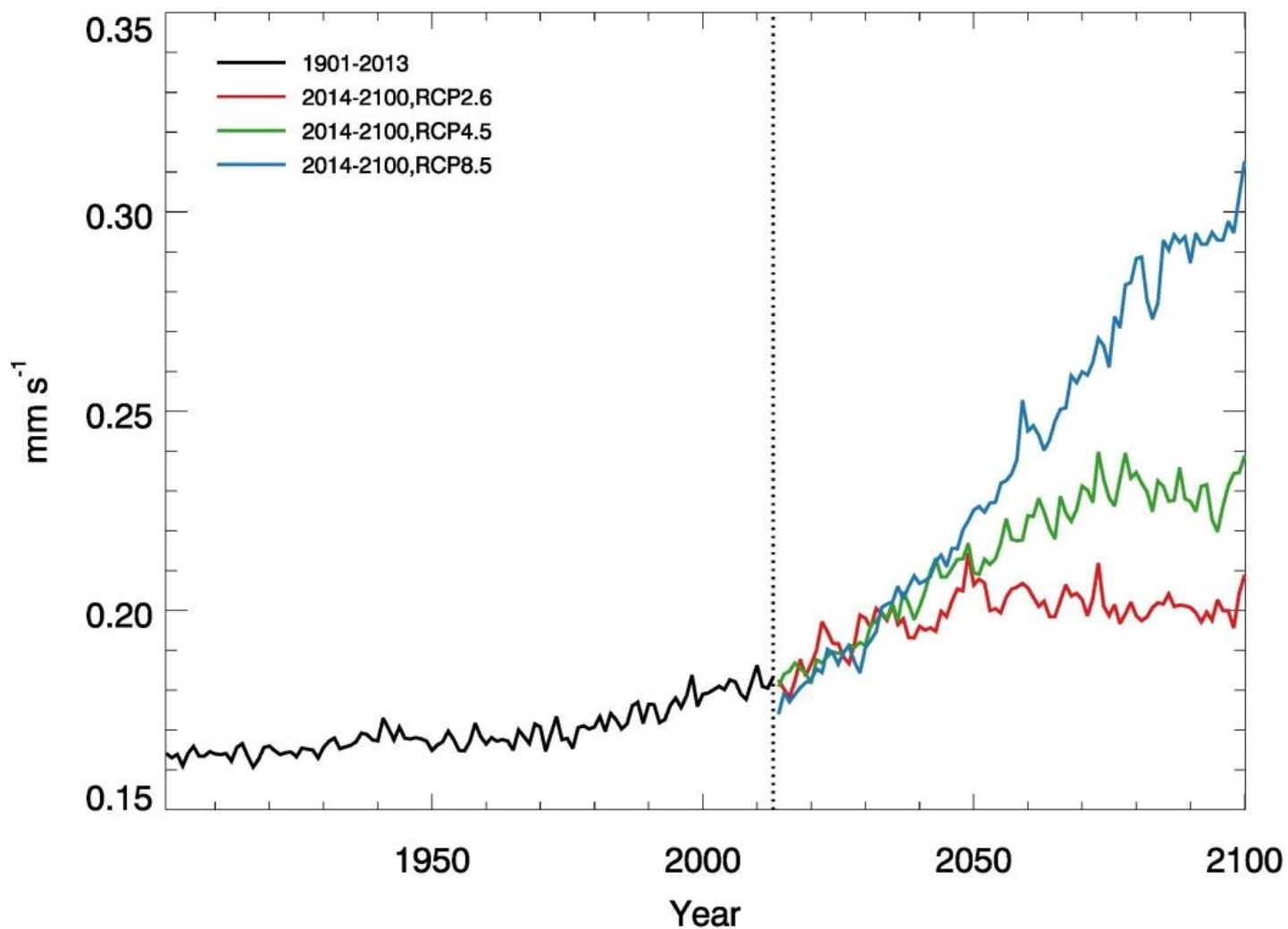
Figure 9. Global mean annual time series of CO deposition velocity (mm s^{-1}) using constant in time, spatially distributed CO concentration data during 1901-2013 (left side of dot line) and under future climate scenarios RCP2.6, RCP4.5 and RCP8.5 during 2014-2100 (right side of dot line)

040

041
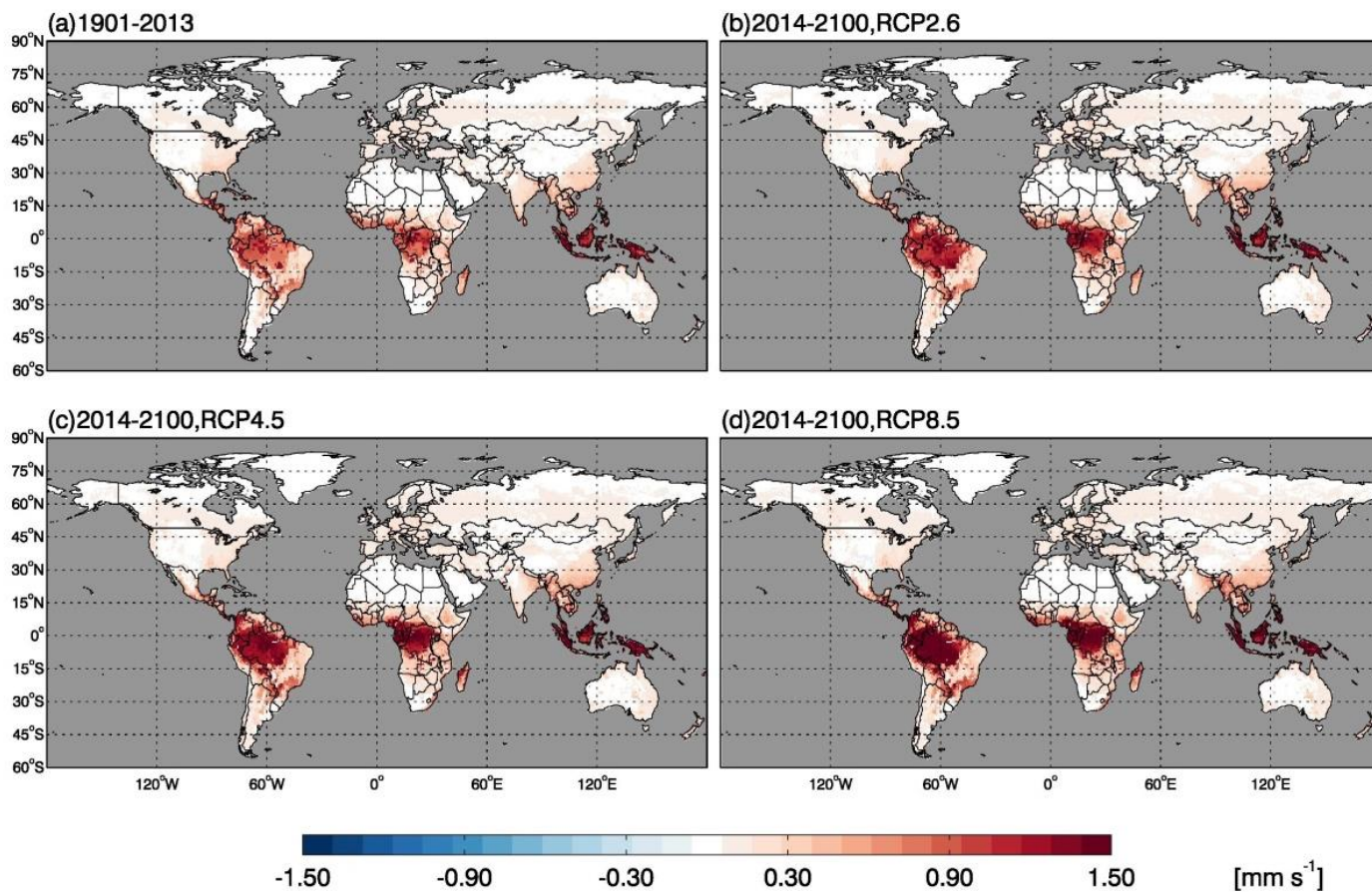
Figure 10. Global annual mean CO deposition velocity using constant in time, spatially distributed CO concentration data (mm s⁻¹) a) during 1901-2013 and b), c), d) under future climate scenarios RCP2.6, RCP4.5 and RCP8.5 during 2014-2100, respectively,

044
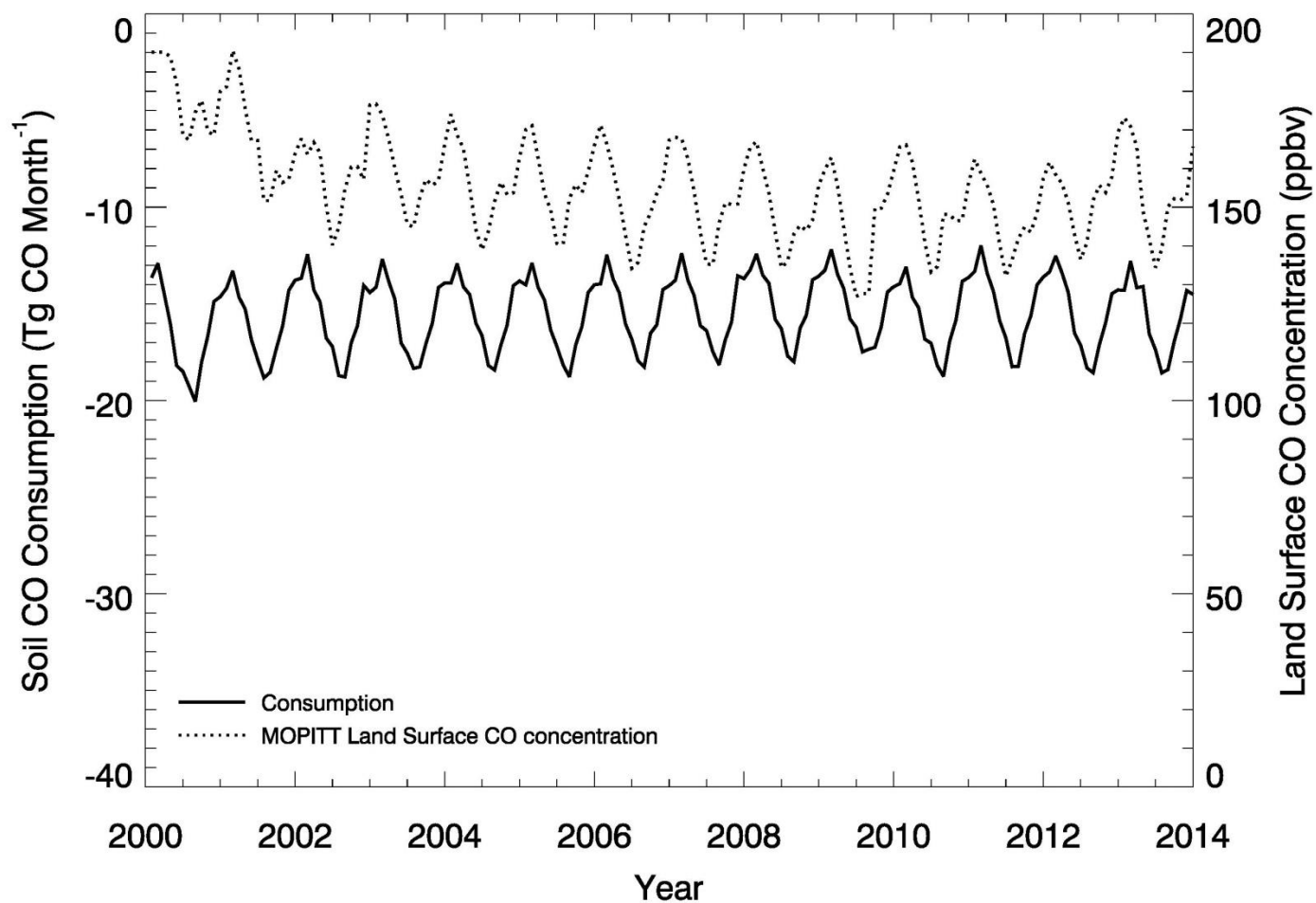
045 **Figure 11.** Global mean monthly time series of MOPITT surface atmospheric CO concentration (ppbv) and soil CO consumption from model simulations E1 (Tg CO mon^{-1})
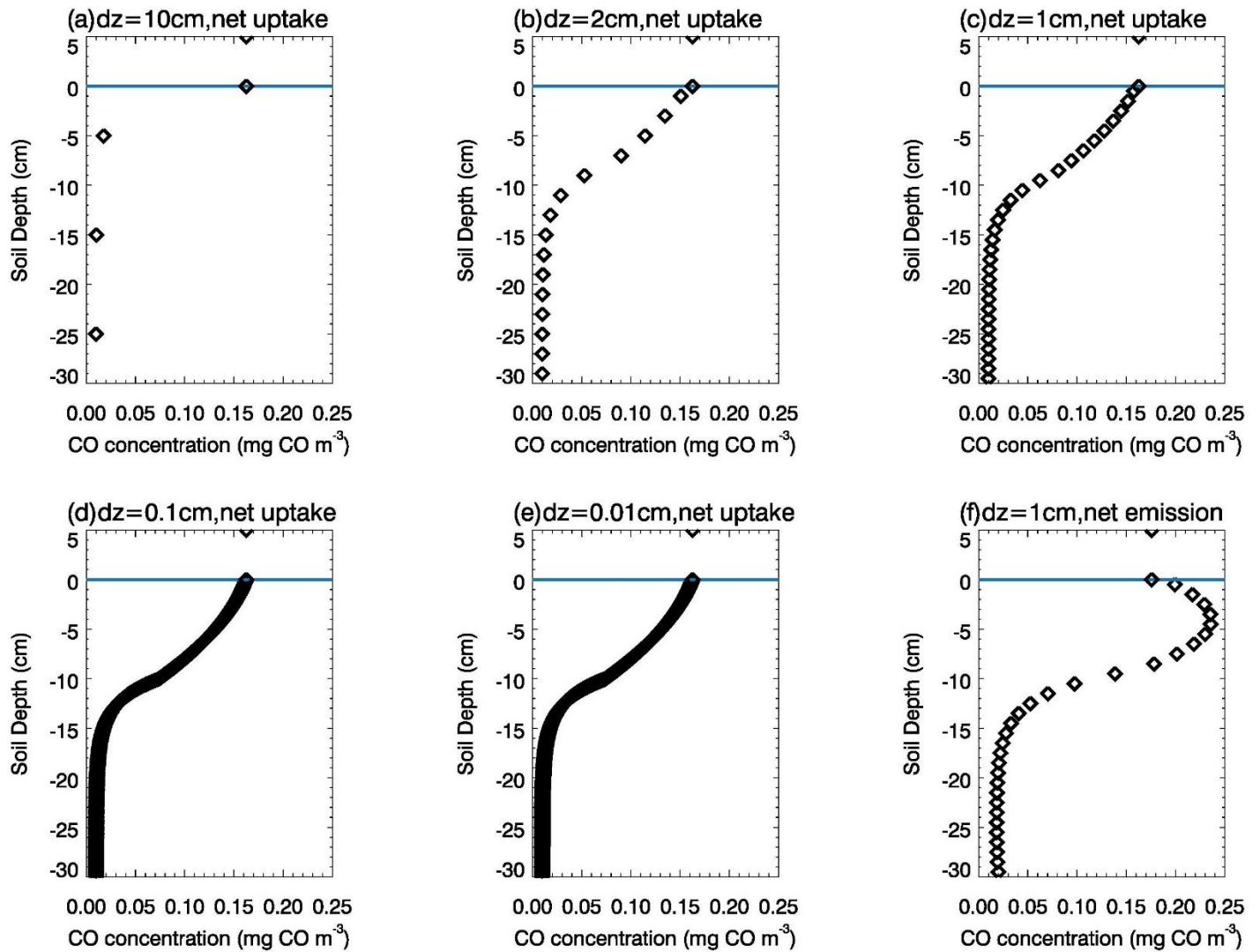
Figure 12. Daily mean vertical soil CO concentration profiles of top 30cm. In soils (depth < 0cm), black diamonds represent the soil CO concentration (mg CO m^{-3}). Above the surface (depth>=0cm), black diamonds represent atmospheric CO concentration. a), b), c), d) and e) are the results from the same day when soil is a net sink of CO but with different layer thickness (dz=10cm, 2cm, 1cm, 0.1cm and 0.01cm respectively); f) is the result from the day when soil is a net source of CO, with dz=1cm.

046
047
048
049
050
051